Identifying short-term and seasonal trends in cave drip water trace element concentrations based on a daily-scale automatically collected drip water dataset

James U.L. Baldini[1], Frank McDermott[2], Lisa M. Baldini[1], Chris J. Ottley[1], Kathryn L. Linge[3], Nicholas Clipson[4], and Kym E. Jarvis[5]

[1]Department of Earth Sciences, University of Durham, Durham, DH1 3LE, UK.
[2]UCD School of Geological Sciences, University College Dublin, Belfield, D4, Ireland.
[3]Curtin Water Quality Research Centre, Curtin University of Technology, GPO Box 41987, Perth WA 6845, Australia.
[4]UCD School of Biology and Environmental Science, University College Dublin, Belfield, D4, Ireland.
[5]Centre for Environmental Policy, Hamilton Building, Imperial College, Silwood Park, Ascot, SL5 7PY, UK.

Abstract

A 13-month long, daily-scale drip water dataset collected by an automatic water sampling device placed in a small cave in Ireland provides evidence for seasonal shifts in hydrochemistry, including a pulse of colloidally-associated elements in the late summer. Ca, Sr, Mg, Na, Ba, P, Cu, Zn, Rb, Y, Cs, U, Th, and Pb concentrations of the collected water samples were determined, and flow rates were also calculated. Alkali and alkali earth metals decreased in concentration during a summer water deficit, whereas colloidally-associated element concentrations increased during the same interval and spiked dramatically in the late summer/early autumn. The observed increase in colloidally-associated element concentrations may have coincided with increased breakdown of soil organic material by microorganisms in the late summer/early autumn, which led to an increased flux of organic colloids in the drip water, or it may relate to increased rates of dry deposition from

cave air. The decrease in alkali and alkali earth metal concentrations in the summer most likely resulted from the addition of dilute water linked to condensation of water vapor above the drip site. Drip water Sr and P concentrations are anticorrelated, and their variation over the study period resembles seasonal trends observed in stalagmite calcite at other sites. Because the Sr minima and P maxima are interpreted as reflecting different phenomena (increased proportion of condensation water relative to karst water, and an increased flux of organic colloids, respectively), the relative timing of these two mechanisms in the past may explain the shifting polarity of their correlation observed in some stalagmite trace element records.

KEYWORDS: stalagmite; palaeoclimate; hydrology; trace elements; drip water; colloids

1. INTRODUCTION

Stalagmites are increasingly used to provide high resolution, accurately dated paleoclimate information for low- to mid-latitude terrestrial areas where few other reliable climate proxies exist. The trace elemental composition of stalagmites shows particular promise as a tool for reconstructing hydrology, rainfall, and bioproductivity; however, our ability to interpret the trace element geochemistry of stalagmites remains limited. Several studies suggest that stalagmite calcite Mg and Sr concentrations effectively constrain paleo-recharge conditions due to a combination of selective leaching, incongruent dissolution, and residence time mechanisms (Roberts, Smart and Baker, 1998; Fairchild et al., 2000; Huang et al., 2001; Treble, Shelley and Chappell, 2003; McDonald, Drysdale and Hill, 2004; McMillan et al., 2005), but many other trace elements remain less well-researched. An early reconnaissance study by Goede and Vogel (1991) measured the concentrations of Na, Mg, Cr, Fe, Co, Zn, Sr, Ba, Sc, Br, La, Au, and U in a Tasmanian stalagmite, but both the temporal resolution and analytical precision were low. Hellstrom and McCulloch (2000) interpreted shifts in Ba, Sr, U, and Mg concentrations in a stalagmite core from New

Zealand as reflecting changes in vegetation amount caused by increasing rainfall. Ba and U shifts were explained by invoking variable soil zone oxidizing conditions caused by temperature-modulated microbial activity that affected Ba and U solubility. However, research has focused predominantly on the trace elements Mg, Sr, and P as paleoclimate proxies, either independently or more commonly to support $\delta^{18}O$ and $\delta^{13}C$ datasets.

Research increasingly suggests that for aquifers lacking dolomite, residence time is the most important control on certain trace element concentrations in drip waters, a relationship that is borne out by drip water studies. A 30-month study of drip water from an Australian cave (Kooringa Cave) demonstrated that the Mg/Ca and Sr/Ca in drip water at this site increased markedly in response to drought conditions, coincident with reduced discharge (McDonald et al., 2004). These increases were interpreted to reflect increased degassing of CO_2 and subsequent calcite precipitation in fissures overlying the cave. This reduces drip water [Ca^{2+}] dramatically, but scarcely affects drip water [Mg^{2+}] and [Sr^{2+}] because of their low partition coefficient in calcite, resulting in elevated ratios. Other cave drip hydrochemical studies have established this 'prior calcite precipitation' (PCP) mechanism as a critical influence on Mg/Ca and Sr/Ca in drip water (Fairchild et al., 2000; Tooth and Fairchild, 2003; Baldini, McDermott and Fairchild, 2006b; McDonald et al., 2007). Tooth and Fairchild (2003) and Baldini et al. (2006b) used long-term monitoring of a wide range of drip types to demonstrate that PCP amounts vary according to site hydrological characteristics. Work in the Edwards aquifer of central Texas suggests that elevated drip water Mg/Ca and Sr/Ca may also reflect increased groundwater residence times and fluid-rock interactions, and are indicative of reduced recharge conditions (Musgrove and Banner, 2004). These elevated ratios could result by either elevated trace element contents or reduced Ca due to PCP.

Microanalytical techniques have successfully resolved annual cycles in stalagmite trace element records (Fairchild et al., 2001; Baldini, McDermott and Fairchild, 2002; Treble et al., 2003) at

spatial resolutions as low as 1 μm, providing a potentially powerful method to build annual-scale chronologies and reconstructing paleoseasonality. Borsato et al. (2007) used micro-X-ray fluorescence spectrometry (μ-XRF) to study Pb, Zn, Fe, Sr, P, Br, Cu, and Y annual cycles at a micron-scale in a stalagmite from Grotta di Ernesto (northern Italy), and assessed the strength of the annual signal for these elements. A Secondary Ionization Mass Spectrometry (SIMS) study of several different speleothems identified annual scale cycles in Mg, Sr, Ba, H, F, Na, and P (Fairchild et al., 2001), suggesting that annual trace element cycles are not uncommon. Of these, Fairchild et al. (2001) suggest that P may have the greatest potential as a paleoclimate proxy due to its role as a nutrient element. This was supported by a study of a modern Australian stalagmite that matched trace element cycles to the instrumental meteorological record and found that P, U, and Mg were the most reliable paleohydrological indicators at that site (Treble et al., 2003). However, the low soil retention capacity for P may have increased the effectiveness of P as a paleohydrological proxy at that site (Treble et al., 2003).

Despite the potential importance of P as a paleoclimate indicator in stalagmite calcite, interpretations have depended largely on inferential relationships with other proxies and calcite petrography; very little information on P concentrations or seasonality in cave drip waters exists. Drip water geochemical work has suggested that several elements, not just P, may be transported bound to colloidal material (any particle between 1 nm and 1 μm in size (Lead and Wilkinson, 2006; Borsato et al., 2007; Fairchild and Hartland, 2010). However, no datasets of P variability in cave dripwaters exist that extend longer than a few months.

Clearly the interest in applying trace element cycles to reconstruct paleoclimate stems largely from the very high resolution achievable using modern microanalytical techniques such as SIMS, μ-XRF, excimer laser ablation inductively coupled plasma mass spectrometry (ELA-ICPMS), and micromilling. However, it is also apparent that drip water sampling studies have not yet matched

the weekly- to monthly- scale temporal resolution possible through microanalytical analyses of speleothem samples, largely because of the logistical difficulties in collecting samples at daily or even weekly intervals. Automated drip loggers have produced very high resolution records of cave drip discharge rates (Sondag et al., 2003; McDonald and Drysdale, 2007; Collister and Mattey, 2008; Hu et al., 2008) and conductivity (Genty and Deflandre, 1998), but long-term drip water trace element monitoring studies have remained at the monthly-scale. Consequently, high-resolution drip water trace element data are critical missing information that would help clarify the links between stalagmite trace element concentrations, climate, aquifer-related processes (e.g., residence time), and crystallographic mechanisms (e.g., calcite growth rate). Here we present the highest resolution long-term major and trace element dataset for a cave drip to date: a daily-scale record of drip water trace element geochemistry extending for almost 14 months for a site in southern Ireland.

2. STUDY SITE

The present study was conducted at Ballynamintra Cave, County Waterford, southern Ireland (52º 7' N, 7º 46' W). Ballynamintra Cave (BC) has one entrance, a total length of 95 m, and is typically separated from the surface by less than two meters of overburden (Fig. 1). The cave is developed in Carboniferous limestone forming an escarpment overlain by a small, well-developed mixed beech and oak wood with substantial undergrowth, and is covered by an organic rich soil typically between 1.0-2.5 m thick, but that may be <1.0 m thick locally. The soil has well-developed 'O' and 'C' horizons (Baldini et al., 2006a). The climate is maritime, the mean temperature for the first 12 months of the study period was 11.3 ºC, and total rainfall 911.0 mm. The mean cave air pCO_2 measured in a previous monitoring study was 0.12% and the humidity was a constant 100% (Baldini et al., 2008). The area is south of the Southern Ireland End Moraine, and thus the traditional interpretation is that the area was unaffected by the Last Glacial Maximum (McCabe, 1987). However, recent research suggests that the Irish Ice Sheet covered almost all of Ireland and

extended out to sea to the south (Ballantyne, McCarroll and Stone, 2006). This debate notwithstanding, the landscape above BC appears free of obvious glacial features and till.

3. METHODS

Drip water samples (n = 174) were collected using a purpose-built automatic water collector placed under one stalactite (30 cm long, 1 cm wide at tip) in BC from November 23, 2004, to January 22, 2006. No stalagmite existed underneath the drip. The water collector consisted of three principal parts: the frame, the drivetrain, and a free-floating bottle holder (Fig. 2). The frame consisted of two acrylic disks, 1 meter in diameter connected by six aluminum rods to form a 'cylinder' 40 cm tall. A 1 cm wide aperture in the top disk, fitted with a small funnel, allowed the drip water to enter into the apparatus, where it fell directly into a pre-cleaned 30 ml low-density polyethylene (LDPE) bottle. The base of the funnel was only 1 cm above the bottle, eliminating potential problems associated with water loss due to splash. The free-floating bottle holder consisted of a central acrylic disk with 32 holes just wide enough to hold 30 ml LDPE bottles, another acrylic disk acting as a support for the bottles, and an aluminum rod extending through the centers of the frame's two acrylic disks and fitted into sockets located in the center of the frame, serving as an axle allowing low-friction rotation of the bottle holder. Metal bolts were installed in the acrylic disk supporting the bottles directly underneath the bottles. The drive train consisted of a motor connected to a timer, which powered the motor and turned a series of gears and belts that rotated the free-floating bottle holder every 48 hours. An electromagnetic switch (positioned on another stationary disk) stopped the motor whenever metal was detected within the switch, ensuring that a bottle was located directly beneath the funnel. All electrical components were coated in plastic to prevent possible short-circuiting caused by condensation. The apparatus was powered by a 12 DCV battery; unexpected voltage drops caused occasional gaps in the record.

Water volumes in the collected bottles were measured gravimetrically, and converted into drip rates in milliliters per minute. Occasionally, the total volume of water discharged by the drip during a 48-hour interval was greater than the volume of the bottle resulting in overflow. In these cases the drip rate is recorded as greater than 0.026 ml minute^{-1}, but the exact figure is unknown. The unfiltered water samples were acidified with Aristar-grade HNO_3, and were analyzed for Sr, Mg, Na, Ba, P, Cu, Zn, Rb, Y, Cs, U, Th, and Pb using an Agilent 7500 inductively coupled plasma mass spectrometer (ICP-MS) at the UK Natural Environmental Research Council's (NERC) ICP Facility (formerly) at Kingston University. Instrumental drift was monitored by running a multi-element standard after every five samples. Appropriate blanks were subtracted from the measured sample values. P measurements were affected by polyatomic interferences at mass 31 derived from the HNO_3 matrix principally due to the formation of $^{14}N^{16}O^{1}H$. These interferences were corrected for by subtracting the appropriate acid blank values from the measured sample values. The corrected P concentrations of selected samples obtained using ICP-MS were replicated successfully at the University of Durham using ICP-AES, an optical technique which thus does not suffer the same problematic interferences as a mass spectrometer for P. Analytical uncertainties were: Mg, Na, Sr, Cu, Ba < 5%, Pb, Rb, P < 10%, U, Zn, Th, Y < 20%, and Cs < 25% (Table 1). Be concentrations were typically very low (<10 ppt) and analytical uncertainty very high (~55%). Be concentration data are presented in Table 1 for reference but are not included in any interpretations. All replicate analyses fell within analytical errors. Drip water Ca concentrations were obtained at University College Dublin using atomic absorption spectrometry (AAS) on a PerkinElmer AAnalyst with <5% analytical uncertainty. Field blanks consisting of the same type of 30ml bottle filled with deionized water were placed near the sampled drip to assess airborne contamination.

Soil and bedrock samples collected above the cave were leached in 7 M HNO_3 for 48 hours. Values for soil and rock used here are the mean values of three replicates for each. Soil and bedrock leachates, as well as a rainwater sample, were analyzed on a Perkin Elmer-Sciex Elan 6000 Q-ICP-

MS at the University of Durham. X-ray diffraction analyses of bedrock, soil, and filtered particulates from drip water were conducted at Trinity College Dublin. SEM and EDX analyses were conducted at University College Dublin. Meteorological data were obtained from the Dungarvan meteorological station approximately 11 km to the SE of Ballynamintra Cave.

4. RESULTS AND DISCUSSION

4.1. Drip Discharge and Chemistry versus Time

The monitored drip demonstrates both short-term (daily-scale) and long-term (seasonal-scale) discharge variability clearly related to rainfall and total evapotranspiration (Fig. 3a, b). Although rainfall was essentially evenly distributed throughout the year, the lowest drip rates occurred from June 1 to September 6, coinciding perfectly with the summer months with the highest evapotranspiration and the lowest calculated water excess (calculated using the extended Thornthwaite equation). Elevated drip rates occurred at a number of times during the rest of the year, but were most common during the winter and spring. The high-resolution sampling permits the detection of storm pulses within the drip rate data. These are characterized by a rapid increase in drip rate (the rising limb of the hydrograph) until peak flow followed by a more gradual return to baseline conditions (the recessional limb). The maximum drip rate during peak flow is unfortunately not always discernable due to bottle overflow, but is at least 0.026 ml min^{-1} (30.0 ml over 48 hours). The recessional limbs typically become asymptotic at around 0.004 ml min^{-1} (5.76 ml day^{-1}) but during the summer period of highest evapotranspiration the drip rate is extremely low (0.00038 ml min^{-1} or approximately four drips per day assuming 0.14 ml per drip). Importantly, the drip never completely ceases, suggesting the presence of a diffuse flow component throughout the year. The drip may therefore exemplify typical two-component flow consisting of: *i)* a short-residence time 'storm' flow probably fed by fractures, and *ii)* more diffuse flow originating from

either intergranular permeability or smaller secondary fractures in the limestone bedrock, although other possibilities are discussed below.

The drip's sensitivity to both seasonal and storm-related recharge conditions permits the characterization of the trace element response to recharge on different scales. The element found in the highest mean concentration (averaged for the entire record) in the drip water was Ca^{2+}, and the rest of the analyzed cations, in order of decreasing concentrations, are: Mg, P, Sr, Zn, Ba, Na, Cu, Pb, Rb, Th, Y, Cs, U, and Be (Table 1). A link between elemental concentration and drip rate is apparent on seasonal timescales (Fig. 3a, b). A gradual decrease in Na, Mg, Ca, Sr, and to a lesser extent Ba and Rb coincides with the decrease in drip rates beginning in June. Concentrations of all of these elements increase again near the end of the summer, just before the September increase in drip rate associated with the gradual reduction in evapotranspiration. Conversely, P, U, Cu, Y, Pb, and Th concentrations increase during this same summer time interval, implying that these two sets of elements are transmitted from the soil and/or bedrock to the cave in a very different manner.

Comparing drip rate to elemental concentrations through the entire record reveals a clear duality in the relationship between elemental concentrations and drip rate (Figs. 4 and 5). At low drip rates, only Na, Mg, Ca, Ba, Rb, and Sr demonstrated reduced concentrations, while the rest of the suite of cations exhibited elevated concentrations. The relationships between drip rate and elemental concentrations are best described by power functions (Fig. 4). The exponent of the best-fit power function describing the relationship between drip rate and concentration provides a measure of the strength and polarity of this relationship, and quantifies the bias of individual elements towards or against specific end-member drip types (e.g., diffuse or fracture flow). A large negative exponent indicates that the element was found at substantially higher concentrations at low rather than high flow, while a large positive exponent indicates the opposite. Exponents close to zero indicate that elemental concentrations did not vary markedly with changing drip rate. However, no element

exhibits a ‘flat’ response to drip rate; all either increase or decrease with increasing drip discharge. The elements whose concentrations appear most independent of drip rate are Ba and Rb, but even these two elements show weak positive and negative relationships with drip rate, respectively (Fig. 4).

4.2. Storm Hydrographs

Drip rates increased in response to intense rainfall events several times during the monitored time period (Fig. 3a, b). All days receiving more than 8.6 mm of rainfall produced a rapid increase in drip rate within one day of the rain event, with the exception of rain events that occurred during the summer period from mid-May to early September, where the drip rate did not respond to rainfall regardless of the rain event’s magnitude. This implies that rainfall was evapotranspired before reaching bedrock fissures capable of transmitting the water to the drip site. All drip rate increases were associated with rain events occurring within the previous 24 hours, but linking flow rate directly to rainfall amount is difficult because the collection bottles often reached maximum capacity during storm pulses thereby preventing the calculation of the maximum discharge rate.

Several storm hydrographs exist in the drip rate record; we have chosen the four most discrete and complete events to analyze in more detail (Fig. 6). These events were initiated by a single short-lived rain event thus allowing more accurate recessional limb characterization than events associated with prolonged or recurrent recharge. The four storm pulses were associated with antecedent 48-hour rainfall amounts of: 1) 11.6 mm, 2) 3.9 mm, 3) 28.1 mm, and 4) 23.5 mm; three out of the four storm-associated hydrographs reached the maximum recordable discharge. Some rainfall did occur after the inception of the storm pulses, and this is reflected in the duration of maximum discharge before the gradual reduction associated with the hydrographs’ recessional limbs. Event 3 in particular was associated with the most prolonged event where rain fell for six

261 days in total, including four days after maximum recordable discharge was reached that delivered
262 37.6 mm of rainfall; this more prolonged recharge event is reflected in the longer duration of this
263 event's maximum discharge compared with the other three (Fig. 6). Although Event 4 (initiating on
264 Dec. 29, 2005), had the second highest antecedent rainfall, the peak discharge was considerably
265 lower than any of the other three. This may be linked to a saturated aquifer or epikarst resulting
266 from several months of water excess diverting recharge associated with discrete events away from
267 the drip site (Sherwin and Baldini, 2011). However, after the summer, the maximum drip discharge
268 rate recorded was only 0.0117 ml min^{-1}, 45% of the maximum routinely reached prior to the
269 summer despite comparable effective rainfall. In particular, 277.6 mm of rainfall fell between the
270 dates of October 7 to November 11, 2005, making this interval the wettest period of our monitoring
271 study, but one associated with a relatively low drip discharge. This suggests that perhaps a change
272 in hydrological routing occurred over the summer period, and that a component of the rapid-flow
273 recharge water was diverted away from the drip site.
274
275 The high resolution water sampling dataset permits the identification of drip water elemental
276 concentration variability on daily timescales, and allows the comparison of this variability to storm-
277 related discharge variability. No element exhibits a consistent change through the duration of all
278 four discrete storm events (Fig. 6). Although some previous studies have detected an initial
279 enrichment in conductivity due to piston flow and the pushing through of 'old' water through the
280 aquifer before the 'new' recharge water (Genty and Deflandre, 1998), no major or trace elements
281 enrichment is observed uniformly during the rising limbs in our dataset. This may result from the
282 relatively small contribution of diffuse water to the overall volume of water discharged during these
283 storm events. If diffuse flow is estimated at approximately 0.005 ml min^{-1} (a maximum value based
284 on summer flow; actual values may be substantially lower as discussed below), then the diffuse
285 flow contributes at most ~20% of the water at maximum discharge, but possibly less because
286 maximum discharge was not quantifiable at the highest flow rates. No element responds similarly to

the four storm events studied in detail, and elemental concentrations vary seemingly independently from drip discharge during all the events. For example, Mg concentrations decrease slightly during and just after storm Event 2, and then gradually increase as the water drains from the aquifer. However, the response was the exact opposite during storm Event 1, and storm Event 3 is characterized by a very large increase in Mg concentrations well after peak discharge is reached, a response very dissimilar to that which occurred during the other three storm pulses. At our drip site, drip water trace and major element geochemistry apparently does not respond consistently or predictably to daily-scale changes in recharge conditions.

4.3. Controls on Drip Water Geochemistry

Concentrations of divalent alkali earth elements and Na are higher during periods of elevated flow and are lowest during the low flow period during the summer (Figs. 3 and 4). This is the opposite of what is typically observed, where increased mean residence time of drip water during intervals of reduced flow increases the concentrations of these elements through increased water/rock interaction (Musgrove and Banner, 2004; Fairchild and Treble, 2009; Fairchild and Hartland, 2010; Schimpf et al., 2011). However, the precipitation of a mineral phase into void spaces prior to drip collection can lower drip water elemental concentrations (Fairchild et al., 2000; Treble et al., 2003; Baldini et al., 2006b; Sherwin and Baldini, 2011). When the mineral phase is calcite, this is known as prior calcite precipitation (PCP), and this removes predominantly Ca from the drip water but also other elements included within the calcite lattice or defect sites. Increased PCP due to decreased drip rates (and increased time for degassing and calcite precipitation) is a possible explanation for the decrease in $[Ca^{2+}]$ observed in the summer months coincident with the decrease in flow rate, however PCP cannot explain the large decreases in the other elements. For example, over the period from May 23 to September 13, $[Ca^{2+}]$ drops by 72% while $[Mg^{2+}]$ drops by 64%; a $[Mg^{2+}]$ decrease of that magnitude compared to the $[Ca^{2+}]$ decrease is impossible via the standard PCP mechanism

because the partition coefficient (K_d) for Mg is too low (dependent on temperature but typically reported as ~0.016 (Huang and Fairchild, 2001; Huang et al., 2001)). A similar argument also applies for Ba, Sr, and Na. This suggests that PCP was not the cause of the observed decreases in concentrations of divalent alkali earth elements and Na during the summer dry period.

Another, more likely, possibility is the mixing of the percolation waters with another, more dilute water. Although the presence of a more dilute water in the shallow aquifer above the cave is unlikely during the high evapotranspiration summer interval, the stalactite from which the drip originates is less than ten meters from the entrance in a section of cave where cave air interacts with outside air frequently (Baldini et al., 2008), possibly leading to condensation on the cave walls and roof. During the summer, when the karst percolation flow was lowest due to increased evapotranspiration, the likelihood of condensation on rock surfaces was also the highest due to warm, high humidity outside air reaching the cave interior and forming condensation on cooler rock surfaces (Sarbu and Lascu, 1997; Dublyanski and Dublyanski, 1998; De Freitas and Schmekal, 2003). A gradual increase in the drip water proportion originating from condensation through the summer could cause the observed gradual reduction in the concentrations of Ca, Mg, Ba, Sr, and Na because the condensation water would be essentially distilled water. Condensation corrosion would cause some dissolved Ca to exist in the water (Tarhule-Lips and Ford, 1998); based on the temperature at the site and likely cave air PCO_2 (based on high resolution PCO_2 monitoring initiated on September 10th, 2005 (Baldini et al., 2008)) the equilibrium [Ca^{2+}] would be 1.09 mmol L^{-1}, almost exactly the value where [Ca^{2+}] values deviate from the decreasing trend previously shared with [Mg^{2+}], [Sr^{2+}], and other alkali and alkali earth metals (Fig. 7). This may represent the addition of condensation water that has reached equilibrium with respect to the calcite-CO_2 system, providing some Ca but negligible amounts of other cations (Fig. 7). The drip site's location in the cave at the boundary between outside air and cave air is ideal for forming large amounts of condensation, and the presence of large quantities of amorphous, microcrystalline calcite masses

('moonmilk') in this area supports this interpretation (Rooney et al., 2010). Moonmilk tends to form in areas experiencing seasonal alterations between condensing and evaporative conditions (Buecher, 1999; Lauriol, Lacelle and Clark, 2004). From a mass balance perspective, dilution by the addition of condensation water is entirely plausible; previous studies at other temperate sites have found condensation rates of between 1 and 15 ml day^{-1} (De Freitas and Schmekal, 2003) and because summer drip rates are so low at our drip site (reaching a minimum of ~0.56 ml day^{-1}, this contribution can easily represent a large part of the collected water. However, no reduction in the concentrations of colloidally-associated trace elements is apparent, and in fact most increased during this interval. An increased flux of these elements through the aquifer during the same time interval may compensate for this dilution effect, or the increased concentrations may be linked with dry deposition of atmospheric particulates within the cave (discussed in Section 4.4).

Concentrations of divalent alkali earth elements and Na respond to seasonal recharge variability as a group and are probably controlled by common mechanisms. The other analyzed elements, mostly transition metals and actinoids, exhibit a very different type of relationship with drip rate, demonstrating increasing concentrations with decreasing discharge. The exponent of the best-fit power function regression line describing the relationship between drip rate and elemental concentrations (Fig. 4) is indicative of each element's tendency to have higher concentrations during low flow. For example, the best-fit power function regression line for Pb is described by:

$$[Pb] = 0.0235(\text{drip rate})^{-0.685} \quad (1)$$

The negative exponent (-0.685) illustrates that Pb concentrations are anticorrelated with drip rate, and a comparison with the exponent describing the relationship between Y concentrations and drip rate (-0.606) demonstrates that Pb concentrations are more anticorrelated with drip rate than Y concentrations, e.g. Pb is slightly more biased towards low flow than Y. These exponents can

365 therefore be used to rank the analysed elements by their affinity for low flow conditions: Th, P, Pb,
366 Cs, Y, Zn, Cu, U, Rb, Ba, Ca, Sr, Mg, and Na. At first glance, it is apparent that elements known to
367 have an affinity for colloidal material in drip water (e.g., Th) have the lowest exponents, whereas
368 the most conservative species (e.g., Na) have the highest exponents. Quantification of an element's
369 affinity for or against adsorption is difficult, but we have used two approaches (Table 1). First, we
370 have considered the mean ocean residence time of an element as being proportional to its sorbtion
371 potential (Fig. 8). The more strongly an element attaches itself to organic or inorganic colloids in
372 the ocean, the shorter its residence time. We also consider the seawater-upper crust partition
373 coefficients (Taylor and McLennan, 1985) as representing adsorption potential (K_y^{SW}); the results
374 are very similar to those using mean residence time in the oceans (Fig. 8). We also develop a
375 'adsorption index', which essentially illustrates how strongly different elements adhere to
376 particulates relative to Th (Table 1), that incorporates both . The elements with a high affinity for
377 adhering onto colloids (quantified using mean ocean residence times and seawater-upper crust
378 partition coefficients) are also most biased towards low flow conditions at our drip site (Fig. 8). The
379 one element deviating from the trend shown on Fig. 8 is P, which is a nutrient element and therefore
380 is recycled in the ocean and has a longer residence time than would otherwise be the case.
381
382 This suggests that either: *i*) these elements are abundant in diffuse flow recharge to the drip
383 throughout the year but concentrations are diluted outside of the summer by high levels of recharge
384 associated with fracture flow or *ii*) that the concentrations are responding to a seasonal increase in
385 elemental flux at the beginning of summer and culminating in late summer/early autumn, coincident
386 with (but independent of) the summer water deficit. Although mechanism *i* may hold partially true,
387 it cannot account for all the variability observed in these elements, because it cannot explain the
388 rapid spike in concentrations beginning in late August, or the decrease in concentrations observed in
389 alkali and alkali earth elements due to the postulated addition of condensation water in the summer.
390 Mechanism *ii* is therefore the preferred interpretation, and this conclusion supports previous

391 research suggesting the existence of an ‘autumnal spike’ in P and other colloidally-associated
392 elements, possibly associated with the seasonal die-back of vegetation. It is possible that organic
393 colloids are released into the aquifer in the late summer and early autumn, and this colloidal
394 material is responsible for the transport much of the P, Cu, Zn, Rb, Y, Cs, U, Th, and Pb into the
395 cave. This is supported by a Cu-Zn-Sr ternary diagram (Fig. 9) which suggests a continuum exists
396 between waters affected predominantly by the bedrock and those affected by soil. Water samples
397 collected in the summer plot further away from the bedrock end member, suggesting that the
398 elevated concentrations of colloidally-associated elements characteristic of the summer, low-
399 recharge samples was more affected by the soil than by the bedrock, consistent with a scenario
400 where drip water chemistry is only affected seasonally by soil colloids when organic colloids are
401 more common (Huang et al., 2001; Fairchild and Treble, 2009).
402
403 **4.4. Possible addition of airborne particles**
404
405 The likely presence of small soil particles in the collected water does not necessarily mean that the
406 particles travelled through the aquifer with the water; the particles could have also been mobilized
407 by airflow in the cave. Air movement through the cave does occur (Baldini et al., 2008), and may
408 transport small particles as described in previous research (Christoforou, Salmon and Cass, 1994;
409 Salmon, Christoforou and Cass, 1994; Pashenko et al., 1996). A study of particulate transport and
410 dry deposition in a man-made cave temple in China found that particles (anthropogenic pollutants in
411 this case) may deposit on surface within the site at rates of up to 19 mg m^{-2} day^{-1} (Christoforou et
412 al., 1994); a rate an order of magnitude smaller than this would still be sufficiently high to greatly
413 affect elemental concentrations in drip water. The water collector was located in an area of the cave
414 known to experience large fluctuations in cave air PCO_2 (Baldini et al., 2008), implying that air
415 movement is substantial at times. Because of the low concentration of elements in the field blanks,
416 it is unlikely that any airborne particles were deposited directly into the sample bottles; rather

deposition may have occurred on the cave walls and roof and then mobilization of these particles in condensed water may have occurred, thus explaining the observed late summer increase. Water travelling through the karst via microfissures may not contact these particles if the discharge point is directly above the stalactite; therefore, dry deposition on the cave roof may occur throughout the year but mobilization may depend on the presence of sufficient condensation water. The seasonality of maximum condensation rates (likely summer for our site) may therefore control the timing of maximum transport of particulates from the cave roof to the drip.

It is worth noting that, although all sample bottles were protected from the cave atmosphere within the automatic collection device, during visits to collect samples the bottles were briefly exposed to the open cave atmosphere, and during this time airborne particles could have entered the collection bottles. This is of particular concern for the samples containing very small amounts of water (some as low as only ~4 drips) and could potentially explain the observed anticorrelation between P, U, Cu, Y, Pb, and Th concentrations and low drip rates. However, blanks consisting of deionized water placed next to the sampler and open to the cave environment over at least one month (compared to just a few minutes for the actual samples) showed no signs of contamination; the concentrations of all elements in these blanks were below detection limits. Also, all samples should demonstrate the effects of airborne particle equally after considering dilution effects; that is, the effects should be linear with respect to drip rate rather than the power function relationship which is observed. This suggests that the any effects of atmospheric particulates were restricted to the summer/late summer period rather than being present throughout the year.

5. IMPLICATIONS

5.1. Colloidally-Associated Trace Elements

443 A number of studies have used trace element concentrations in stalagmites as palaeoclimate proxies
444 or, if annual trace element cycles were present, as chronological tools (Baldini et al., 2002; Treble et
445 al., 2003; McMillan et al., 2005; Johnson et al., 2006). High resolution studies of stalagmites
446 typically interpret elevated concentrations of many colloidally-associated elements as characteristic
447 of autumnal deposited calcite; these elevated concentrations also often coincide with darker, UV-
448 fluorescent calcite (Fairchild et al., 2001; Richter et al., 2004; Borsato et al., 2007). Interestingly,
449 the distribution through the year of normalized concentrations of colloidally-associated trace
450 elements in the BC drip water match remarkably well with inferred seasonality in the same
451 elements from a stalagmite collected from Grotta di Ernesto, northern Italy, analyzed at a very high
452 resolution using synchrotron radiation induced fluorescence. Despite differences in climate, soil
453 type, altitude, hydrology, bedrock, and cave environmental characteristics, the normalized
454 concentrations between BC drip water and Grotta di Ernesto stalagmite calcite match remarkably
455 well, suggesting a common mechanism of transport for these elements (Fig. 10). Based on the
456 association of the colloidally-associated trace elements in the Ernesto stalagmite with UV-
457 fluorescent subannual layers, Borsato et al. (2007) suggested that these elements were transported to
458 the stalagmite with colloidal material during periods of more intense rainfall in the autumn,
459 combined with increased organic matter breakdown by microbes, an interpretation supported by
460 other studies (e.g., (Schimpf et al., 2011)). This interpretation is partially supported by our data,
461 which does show an increase in these elements in the late summer/early autumn, but this elemental
462 concentration increase is not associated with an increase in drip rate associated with rapid recharge.
463 In fact, increases in drip rate in the BC record are associated with decreases in concentrations of
464 potentially colloidally-associated TEs. This suggests that at this one site (BC) the ‘autumnal spike’
465 in concentration of these TEs is largely dependent on soil biological processes rather than
466 mechanical entrainment of particles. However, because soil may contain elevated concentrations of
467 these elements, mechanical entrainment of soil particulates of any size could occur at other caves,
468 and possibly at other drip sites within BC as well. The contribution of cave air particulates at certain

times of the year may also play a role, as of yet not well quantified but that needs to be researched further.

5.2. Alkali and Alkali Earth Element Variability

The BC drip water dataset and the Grotta di Ernesto stalagmite both exhibit decreases in Sr concentrations coinciding with increases in colloidally-associated elements. Borsato et al. (2007) suggested that in their stalagmite the seasonal Sr decreases may have resulted from increased competition for non-lattice sites due to a seasonal increase in other TE associated with the 'autumnal spike'. Although this is a very likely scenario, crystallographic effects cannot explain the remarkably similar decrease observed in the drip water dataset from BC. In the drip water dataset, this must therefore reflect differences in the supply and/or mode of transport of Sr compared to P, Cu, Zn, Rb, Y, Cs, U, Th, and Pb. The similarity in behavior of Sr to Ca, Mg, Ba, and Na suggests that controls on these elements are similar. At our site, colloidally-associated elements have higher concentrations at low flow and reflect a greater soil influence, whereas Sr, Ca, Mg, Ba, and Na all have higher concentrations at high flow and reflect a greater bedrock influence (Fig. 9). However, because [Ca^{2+}] variability tracks [Sr^{2+}] (as well as [Mg^{2+}], [Ba^{2+}], and [Na^{+}]), any calcite deposition may not reflect the annual trough in drip water [Sr^{2+}] observed in the present study because Sr incorporation into calcite is controlled not by Sr concentrations, but rather the ratio of drip water [Sr^{2+}] to [Ca^{2+}] according to:

$$\left(\frac{[TE]}{[Ca^{2+}]}\right)_{calcite} = \left(\frac{[TE]}{[Ca^{2+}]}\right)_{water} \times D_{TE} \quad (2)$$

where D_{TE} is the distribution coefficient for the element, [TE] is the concentration of the trace element, and [Ca^{2+}] is the concentration of calcium. Therefore, drip water [TE]/[Ca^{2+}] ratios can be

used to predict calcite TE concentrations, assuming that D_{TE} does not vary through the year (potentially an oversimplification – discussed below). $[Sr^{2+}]/[Ca^{2+}]$ does not display the same pronounced decrease in the summer as $[Sr^{2+}]$ because $[Ca^{2+}]$ is decreasing simultaneously (Fig. 11). Therefore, seasonally variable drip water $[Sr^{2+}]$ on its own is unlikely to result in an annual cycle in any deposited calcite. Rather, crystallographic effects associated with competition for non-lattice sites (Borsato et al., 2007), combined with lower drip water $[Sr^{2+}]$, could result in the observed trough in Sr coincident with the colloidally-associated TE in the stalagmite from Grotta di Ernesto (Borsato et al., 2007). This same relationship between alkali earth elements (e.g., Sr) and colloidally-associated elements is also observed at Heshang Cave, China, where Mg, Sr, and Ba, are anticorrelated with U (Johnson et al., 2006). At this site, the seasonal U concentration maximum (and Mg, Sr, and Ba concentration minima) again occurs coincident with darker calcite which contains abundant organic material, further suggesting that the concentrations are linked to bioproductivity changes. The link to a soil bioproductivity control on certain elements is further reinforced by research on stalagmites from St. Michaels Cave, Gibraltar, demonstrating that Na, Ba, Sr, and Mg are anticorrelated with P, whose concentrations are highest in light columnar calcite and lowest in dark calcite (Mattey et al., 2008), the opposite of the usual relationship between petrography and P. Calcite growth at this site is largely modulated by cave air P_{CO_2}; rapid growth during the summer (when the cave is well-ventilated) is believed to produce the dark calcite, whereas slower winter growth may result in the light columnar calcite. The P concentration peaks are coincident with the lighter calcite because its deposition coincides with the highest soil bioproductivity, during the winter at this Mediterranean site (Mattey et al., 2008).

However, this seasonal anticorrelation between alkali (and alkali earth) and potentially colloidally-associated TE is not universal and does vary from site to site. For example, a high resolution ELA-ICPMS study of an Australian stalagmite showed that in this chemically laminated sample seasonal Sr variability correlated positively with both P and U (Treble et al., 2003), two elements

anticorrelated with Sr in the Grotta di Ernesto stalagmite and the BC drip water. This inter-site variability may arise from the very different types of soil and climate between sites. Additionally, it is possible that the Australian stalagmite is not affected by colloidal material, and that both the P and U are linked to soil redox variability rather than changes in colloidal flux (Treble et al., 2003).

5.3. P and U Variability

Although the concept of distribution coefficients is useful for modeling the incorporation of certain elements into calcite, the approach is limited to those elements tending to exist as non-complexed dissolved ions in drip water. Both P and U are among the TE demonstrating the most potential for palaeoclimate reconstructions, but both are typically found in carbonate groundwaters as orthophosphate and uranyl ions, respectively, rather than simple dissolved ions (House, 1987; Sandino and Bruno, 1992; Cheng et al., 2007). Orthophosphate (PO_4^{2-}) and uranyl (UO_2^{+}) ions are likely to adsorb strongly to mineral and organic material and in practice rarely exist as free aqueous ions in carbonate groundwaters (Drever, 1997). In addition to the water collected daily by the automatic water sampler, integrated monthly drip water samples were collected at four other drip sites in BC. This water was characterized by extremely low (generally below detection limits) free orthophosphate concentrations but higher unreactive phosphorus concentrations (solubilized by using a strong HNO_3-H_2SO_4 digestion), indicative of a non-dissolved phase. Large volumes of these waters were filtered using 0.45 micron filter paper to isolate the particulate phase, though any colloidal material would have passed through the filter. X-ray diffractometry of the residue left on the filter paper revealed the presence of soil-derived hydroxyapatite, which could contribute some of the P apparent in the drip water. However, EDX mapping and spot analyses suggested the presence of another P-rich non-silicate phase (Fig. 12). Spot analyses suggest that these particles also have high carbon content, so they are probably organic material entrained from the soil. It is difficult to perform mass balance calculations based exclusively on these findings because much of

547 the colloidal material may have passed through the filter and been lost, but the EDX and XRD data
548 do indicate that both mineral and non-mineral (i.e., organic) particulate phases existed in the drip
549 water in at least one drip site within BC. Huang et al. (2001) used a mass balance argument based
550 on the C/P ratio of soil organic matter to argue that at Grotta di Ernesto the seasonal P concentration
551 peak could not arise through organic material incorporation alone, and that other sources must also
552 exist. This was later supported by Mason et al. (2007) who identified several phases containing P in
553 a stalagmite from Grotta di Ernesto, including phosphate ions located within defect sites, monetite
554 ($CaHPO_4$), and another unidentified crystalline phase. However, no crystalline phases were
555 associated with phosphate in another stalagmite from a different site (Grotte de Clamouse, France),
556 and the authors suggested that in that stalagmite all P is present as phosphate ions in calcite defect
557 sites (Mason et al., 2007).
558
559 If free orthophosphate or uranyl ions are present in drip water, these will probably co-precipitate
560 with calcite because both ions adsorb strongly to calcite; therefore PCP would probably lead to
561 reduced values in both P and U (Johnson et al., 2006). However, both orthophosphate and uranyl
562 ions form carbonate complexes in alkaline groundwaters typical of karstic regions, and also adsorb
563 strongly onto organic and inorganic particles (Wood, 1990; Cheng, Barnett and Roden, 2004; Luo
564 and Byrne, 2004; Quinn, Byrne and Schijf, 2006), so if colloidal particulate material is present in
565 the drip water, this may exert a more powerful control on stalagmite U and P concentrations than
566 PCP. Therefore, variability in the concentrations of these two elements in the BC drip water dataset
567 are probably linked to varying amounts of colloidal material in the drip water (either transported
568 through the karst or as entrained atmospheric particulates that had settled on the cave roof), and the
569 spike in late summer/early autumn could result from increased amounts of organic colloids in the
570 drip water due to increased soil microbial degradation of organic material. This increase in TE
571 concentrations is not associated with a drip rate increase, suggesting that the colloids, if present, are

not inorganic as these would presumably require an increase in flow rate for transport rather than simply a change in soil organic matter and microbial content.

5.4. Comparison with Ballynamintra Cave Stalagmite BA99-4

Previously published research used secondary ion mass spectrometry (SIMS) to demonstrate the presence of annual geochemical cycles in a stalagmite (BA99-4) sampled from BC (Fairchild et al., 2001). Unfortunately no drip water geochemical data exist for this previously collected sample, but the drip feeding the stalagmite was observed to stop flowing during the summer (Fairchild et al., 2001), similar with our observations at our high-resolution water collecting site (demonstrating drip rates as low as 4 drips per day during the summer) and suggesting that the two drips are fed by a similar type of hydrology. Stalagmite BA99-4 was also found to have visible and UV annual banding, and that the dark UV-fluorescent bands corresponded with an increase in concentration of certain TE, including P which was found to vary antipathetically with Mg (Fairchild et al., 2001), consistent with our high resolution drip data. However, Sr varied both in and out of phase with P in the stalagmite, whereas Sr was anticorrelated with P in our drip water dataset. This difference suggests that if Sr concentrations are indeed lowered in stalagmite calcite due to increased competition for non-lattice defect sites during periods of increased colloidal flux, then occasionally this colloidal flux is insufficient to fully saturate these sites, and that Sr is able to take advantage of the remaining sites. If the autumnal flush of colloidally-associated TE (including P) occurs approximately at the same time every year regardless of the amount of rainfall, an unusually wet summer could produce elevated Sr in the stalagmite coincident with the autumnal flush. Controls on Sr and on colloidally-associated TE are therefore potentially independent and their seasonality could shift through time. The comparison between our drip water dataset and the previously analyzed stalagmite does further suggest that complex, and potentially independent, controls on different types of elements exist at BC. Further high-resolution water sampling studies at other sites

598 are needed to investigate the controls on drip water elemental content, and whether these controls
599 are universal or site-specific.
600
601 **6. CONCLUSIONS**
602
603 The daily-scale cave drip water data presented here have identified a seasonal spike in the
604 concentration of colloidally-associated elements in drip water occurring in the late summer/early
605 autumn. This may relate to increased decomposition of soil organic matter producing more organic
606 colloidal material, which is then transported to the drip site within the cave. It may also relate to
607 increased movement of cave air particulates into the water sampling bottles. If flushing is the cause,
608 the flushing event did not correspond with increased drip rates or intense rainfall, suggesting that at
609 our site increased mechanical transport of the colloidal material is not the principal driver of the
610 flushing event. However, not all TEs responded to the autumnal flushing event proportionally, and
611 two clearly different groups exist. Alkali and alkali earth element (Mg, Na, Ca, Sr, and Ba)
612 concentrations decreased with decreasing drip rate coincident with the 'autumnal spike'.
613 Conversely, concentrations of P, Cu, Zn, Rb, Y, Cs, U, Th, and Pb all increased at this time,
614 suggesting the two sets of elements are controlled by different mechanisms. The TEs discussed here
615 are found in drip water either adsorbed to particulate matter, as part of the principal chemical
616 structure of small particles, as a dissolved phase, or more likely a combination of all three. Alkali
617 and alkali earth element concentrations are instead moderated by: *i*) interactions with the carbonate
618 bedrock and *ii*) dilution through the addition of condensation water during the summer.
619 Condensation contributions to the drip water budget are rarely considered in the literature; however,
620 our results suggest that condensation may potentially affect drip hydrochemistry and ultimately
621 stalagmite calcite seasonally at certain drip sites. Our research also suggests that the autumnal spike
622 at BC results from either *i*) the flushing of organic colloidal material through the aquifer, thus only
623 significantly increasing TE concentrations associated with this phase (i.e., P, Cu, Zn, Rb, Y, Cs, U,

624 Th, and Pb) or *ii*) the accumulation of airborne particulate matter on cave walls followed by
625 transport by condensation-derived water into the sample bottles.
626
627 A broad spectrum of particle sizes and types exist in cave drip waters that may ultimately be
628 incorporated into secondary calcites, which, particularly when considered together with dissolved
629 phases, greatly complicate the interpretation of trace elements in stalagmites. It is now appreciated
630 that many stalagmites are chemically laminated and that concentrations of a broad suite of trace
631 elements vary on a seasonal basis. The concentrations of different trace elements in stalagmites may
632 correlate positively or negatively at different sites. This may partially result from site-to-site
633 variability in the relative importance of non-dissolved mineral or organic material present in the
634 drip water feeding the stalagmite. High resolution trace element analyses typically attempt to avoid
635 areas of obvious non-carbonate material in a stalagmite, but because this material exists across a
636 spectrum of sizes ranging from macroscopic to colloidal, the particulates may not always be visible
637 or avoidable. Therefore this material, particularly if colloidal and difficult to identify visually, will
638 play an important role in determining the structure of a TE profile through a stalagmite. At our drip
639 site, concentrations of Sr and colloidally-associated TE appear seasonally anticorrelated, though we
640 propose that this relationship's polarity may switch at other sites characterized by the absence of
641 particulate material (colloidal or otherwise) in the drip water. For example, Sr and P concentrations
642 are often observed to anticorrelate in stalagmite geochemical datasets; this could result from a
643 seasonal flux of colloids increasing stalagmite P concentrations while Sr concentrations are
644 simultaneously reduced by increased competition for non-lattice sites, crystal surface poisoning,
645 and a reduction in growth rate affecting Sr incorporation. Conversely, at some cave sites P and Sr
646 are positively correlated; this could result from the absence of colloidal material in the drip feeding
647 the stalagmite, which reduces competition for non-lattice sites and crystallographic effects. In this
648 case dissolved P and Sr concentrations in the drip water may co-vary and determine the P and Sr
649 content in the stalagmite. Perhaps the concentration of an element rarely found in a dissolved phase

(e.g., Th) could be used to quantify the relative importance of colloidal material in stalagmite samples.

Trace elemental concentrations in stalagmites are a powerful palaeoclimatic tool when used on their own or in combination with stable isotope records. This research further supports the observation that stalagmites have seasonal cycles in the concentrations of many TE, and that this cycle is partially modulated by seasonal variability in drip water dissolved and colloidal chemical phases. The concentrations of certain trace elements are controlled by residence time in the aquifer and by drip water/bedrock interactions and therefore could provide important information regarding water availability. This research supports prior suggestions that the peak in colloidally-associated TE concentrations occurs sometime in the late summer/early autumn, either associated with increased soil organic matter degradation or with increased transport of cave air-derived dry deposition, and thus further establishes these elements as useful tools for constructing annually resolved geochemistry-based chronologies. Additionally, this research emphasizes the potential importance of two previously poorly researched mechanisms that could partially control trace element concentrations in stalagmite calcite: dry deposition from cave air and drip water dilution due to condensation-derived water.

7. ACKNOWLEDGEMENTS

This research was funded by Enterprise Ireland Basic Research Grant 3750/92201/R8965. We thank Dr Vanessa Johnston for help with fieldwork, and the landowners for providing access to the site. The technical staff at the UCD School of Physics are thanked for assistance with the construction of the automatic drip sampling device. Prof. Ian Fairchild and two anonymous reviewers are thanked for helpful comments that improved the manuscript.

References:

Baldini J.U.L., Baldini L.M., McDermott F., Clipson N. (2006a) Carbon dioxide sources, sinks, and spatial variability in shallow temperate zone caves: evidence from Ballynamintra Cave, Ireland. *J Cave Karst Stud* **68**, 4-11.

Baldini J.U.L., McDermott F., Fairchild I.J. (2002) Structure of the 8200-year cold event revealed by a speleothem trace element record. *Science* **296**, 2203-2206.

Baldini J.U.L., McDermott F., Fairchild I.J. (2006b) Spatial variability in cave drip water hydrochemistry: Implications for stalagmite paleoclimate records. *Chem. Geol.* **235**, 390-404.

Baldini J.U.L., McDermott F., Hoffmann D.L., Richards D.A., Clipson N. (2008) Very high-frequency and seasonal cave atmosphere P_{CO2} variability: Implications for stalagmite growth and oxygen isotope-based paleoclimate records. *Earth Planet. Sci. Lett.* **272**, 118-129.

Ballantyne C.K., McCarroll D., Stone J.O. (2006) Vertical dimensions and age of the Wicklow Mountains ice dome, Eastern Ireland, and implications for the extent of the last Irish Ice Sheet. *Quaternary Sci Rev* **25**, 2048-2058.

Borsato A., Frisia S., Fairchild I.J., Somogyi A., Susini J. (2007) Trace element distribution in annual stalagmite laminae mapped by micrometer-resolution X-ray fluorescence: implications for incorporation of environmentally significant species. *Geochim. Cosmochim. Acta* **71**, 1494-1512.

Buecher R.H. (1999) Microclimate study of Kartchner Caverns, Arizona. *J Cave Karst Stud* **61**, 108-120.

Cheng T., Barnett M.O., Roden E.E. (2004) Uranium (VI) adsorption to goethite-coated sand: Effects of phosphate. *Abstr Pap Am Chem S* **227**, U1112-U1112.

Cheng T., Barnett M.O., Roden E.E., Zhunag J.L. (2007) Reactive transport of uranium(VI) and phosphate in a goethite-coated sand column: An experimental study. *Chemosphere* **68**, 1218-1223.

Christoforou C.S., Salmon L.G., Cass G.R. (1994) Deposition of Atmospheric Particles within the Buddhist Cave Temples at Yungang, China. *Atmos. Environ.* **28**, 2081-2091.

Collister C., Mattey D. (2008) Controls on water drop volume at speleothem drip sites: An experimental study. *J Hydrol* **358**, 259-267.

De Freitas C.R., Schmekal A. (2003) Condensation as a microclimate process: Measurement, numerical simulation and prediction in the Glowworm Cave, New Zealand. *Int J Climatol* **23**, 557-575.

Drever J.I., 1997. The Geochemistry of Natural Waters. Prentice-Hall, Inc., Upper Saddle River, N.J.

Dublyanski V.N., Dublyanski Y.V. (1998) The problem of condensation in karst studies. *J Cave Karst Stud* **60**, 3-17.

Fairchild I.J., Baker A., Borsato A., Frisia S., Hinton R.W., McDermott F., Tooth A.F. (2001) Annual to sub-annual resolution of multiple trace-element trends in speleothems. *J. Geol. Soc. London* **158**, 831-841.

Fairchild I.J., Borsato A., Tooth A.F., Frisia S., Hawkesworth C.J., Huang Y., McDermott F., Spiro B. (2000) Controls on trace element (Sr-Mg) compositions of carbonate cave waters: implications for speleothem climatic records. *Chem. Geol.* **166**, 255-269.

Fairchild I.J., Hartland A. (2010) Trace element variations in stalagmites: controls by climate and by karst system processes. *EMU Notes in Mineralogy* **10**, 259-287.

Fairchild I.J., Treble P.C. (2009) Trace elements in speleothems as recorders of environmental change. *Quaternary Sci Rev* **28**, 449-468.

Genty D., Deflandre G. (1998) Drip flow variations under a stalactite of the Père Noël cave (Belgium). Evidence of seasonal variations and air pressure constraints. *J Hydrol* **211**, 208-232.

Goede A., Vogel J.C. (1991) Trace element variations and dating of a Late Pleistocene Tasmanian speleothem. *Palaeography, Palaeoclimatology, Palaeoecology* **88**, 121-131.

Hellstrom J.C., McCulloch M.T. (2000) Multi-proxy constraints on the climatic significance of trace element records from a New Zealand speleothem. *Earth Planet. Sci. Lett.* **179**, 287-297.

House W.A. (1987) Inhibition of calcite crystal growth by inorganic phosphate. *J. Colloid Interface Sci.* **119**, 505-511.
Hu C.Y., Henderson G.M., Huang J.H., Chen Z.H., Johnson K.R. (2008) Report of a three-year monitoring programme at Heshang Cave, Central China. *Int J Speleol* **37**, 143-151.
Huang Y., Fairchild I.J. (2001) Partitioning of Sr^{2+} and Mg^{2+} into calcite under karst-analogue experimental conditions. *Geochim. Cosmochim. Acta* **65**, 47-62.
Huang Y., Fairchild I.J., Borsato A., Frisia S., Cassidy N.J., McDermott F., Hawkesworth C.J. (2001) Seasonal variations in Sr, Mg and P in modern speleothems (Grotta di Ernesto, Italy). *Chem. Geol.* **175**, 429-448.
Johnson K.R., Hu C., Belshaw N.S., Henderson G.M. (2006) Seasonal trace-element and stable-isotope variations in a Chinese speleothem: The potential for high-resolution paleomonsoon reconstruction. *Earth Planet. Sci. Lett.* **244**, 394-407.
Lauriol B., Lacelle D., Clark I.D. (2004) Seasonal isotopic imprint in moonmilk from Caverne de l'Ours (Quebec, Canada): implications for climatic reconstruction. *Can. J. Earth Sci.* **41**, 1411-1423.
Lead J.R., Wilkinson K.J. (2006) Aquatic colloids and nanoparticles: Current knowledge and future trends. *Environ Chem* **3**, 159-171.
Luo Y.R., Byrne R.H. (2004) Carbonate complexation of yttrium and the rare earth elements in natural waters. *Geochim. Cosmochim. Acta* **68**, 691-699.
Mason H.E., Frisia S., Tang Y., Reeder R.J., Phillips B.L. (2007) Phosphorus speciation in calcite speleothems determined from solid-state NMR spectroscopy. *Earth Planet. Sci. Lett.* **254**, 313-322.
Mattey D., Lowry D., Duffet J., Fisher R., Hodge E., Frisia S. (2008) A 53 year seasonally resolved oxygen and carbon isotope record from a modem Gibraltar speleothem: Reconstructed drip water and relationship to local precipitation. *Earth Planet. Sci. Lett.* **269**, 80-95.
McCabe A.M. (1987) Quaternary deposits and glacial stratigraphy in Ireland. *Quaternary Sci Rev* **6**, 259-299.
McDonald J., Drysdale R. (2007) Hydrology of cave drip waters at varying bedrock depths from a karst system in southeastern Australia. *Hydrol Process* **21**, 1737-1748.
McDonald J., Drysdale R., Hill D. (2004) The 2002-2003 El Nino recorded in Australian cave drip waters: Implications for reconstructing rainfall histories using stalagmites. *Geophys. Res. Lett.* **31**, 1-4.
McDonald J., Drysdale R., Hill D., Chisari R., Wong H. (2007) The hydrochemical response of cave drip waters to sub-annual and inter-annual climate variability, Wombeyan Caves, SE Australia. *Chem. Geol.* **244**, 605-623.
McMillan E.A., Fairchild I.J., Frisia S., Borsato A., McDermott F. (2005) Annual trace element cycles in calcite-aragonite speleothems: evidence of drought in the western Mediterranean 1200-1100 yr BP. *Journal of Quaternary Science* **20**, 423-433.
Musgrove M., Banner J.L. (2004) Controls on the spatial and temporal variability of vadose dripwater geochemistry: Edwards Aquifer, central Texas. *Geochim. Cosmochim. Acta* **68**, 1007-1020.
Pashenko S., Dublyansky Y., Andreichuk V., Pahenko E. (1996) Transformation of fractal atmospheric aerosol moving through natural cave. *J. Aerosol Sci.* **27**, S127-S128.
Quinn K.A., Byrne R.H., Schijf J. (2006) Sorption of yttrium and rare earth elements by amorphous ferric hydroxide: Influence of solution complexation with carbonate. *Geochim. Cosmochim. Acta* **70**, 4151-4165.
Richter D.K., Gotte T., Niggemann S., Wurth G. (2004) REE^{3+} and Mn^{2+} activated cathodoluminescence in lateglacial and Holocene stalagmites of central Europe: evidence for climatic processes? *Holocene* **14**, 759-767.
Roberts M.S., Smart P.L., Baker A. (1998) Annual trace element variations in a Holocene speleothem. *Earth Planet. Sci. Lett.* **154**, 237-246.
Rooney D.C., Hutchens E., Clipson N., Baldini J., McDermott F. (2010) Microbial community diversity of moonmilk deposits at Ballynamintra Cave, Co. Waterford, Ireland. *Microbial Ecology* **60**, 753-761.

Ryder P.F. (1989) Caves in County Waterford, October 1988. *Irish Speleology* **13**, 45-50.
Salmon L.G., Christoforou C.S., Cass G.R. (1994) Airborne pollutants in the Buddhist cave temples at the Yungang Grottoes, China. *Environmental Science & Technology* **28**, 805-811.
Sandino A., Bruno J. (1992) The Solubility of $(UO_2)_3(PO_4)_2 \cdot 4H_2O_{(S)}$ and the formation of U(VI) phosphate complexes: their influence in uranium speciation in natural waters. *Geochim. Cosmochim. Acta* **56**, 4135-4145.
Sarbu S.M., Lascu C. (1997) Condensation corrosion in Movile Cave, Romania. *J Cave Karst Stud* **59**, 99-102.
Schimpf D., Kilian R., Kronz A., Simon K., Spötl C., Wörner G., Deininger M., Mangini A. (2011) The significance of chemical, isotopic, and detrital components in three coeval stalagmites from the superhumid southernmost Andes (53°S) as high-resolution palaeo-climate proxies. *Quaternary Sci Rev* **30**, 443-459.
Sherwin C.M., Baldini J.U.L. (2011) Cave air and hydrological controls on prior calcite precipitation and stalagmite growth rates: Implications for palaeoclimate reconstructions using speleothems. *Geochim. Cosmochim. Acta* **75**, 3915-3929.
Sondag F., van Ruymbeke M., Soubies F., Santos R., Somerhausen A., Seidel A., Boggiani P. (2003) Monitoring present day climatic conditions in tropical caves using an Environmental Data Acquisition System (EDAS). *J Hydrol* **273**, 103-118.
Tarhule-Lips R.F.A., Ford D.C. (1998) Condensation corrosion in caves on Cayman Brac and Isla de Mona. *J Cave Karst Stud* **60**, 84-95.
Taylor S.R., McLennan S.M., 1985. The Continental Crust: its Composition and Evolution. Blackwell, Oxford.
Tooth A.F., Fairchild I.J. (2003) Soil and karst aquifer hydrological controls on the geochemical evolution of speleothem-forming drip waters, Crag Cave, southwest Ireland. *J Hydrol* **273**, 51-68.
Treble P., Shelley J.M.G., Chappell J. (2003) Comparison of high resolution sub-annual records of trace elements in a modern (1911-1992) speleothem with instrumental climate data from southwest Australia. *Earth Planet. Sci. Lett.* **216**, 141-153.
Wood S. (1990) The aqueous geochemistry of the rare-earth elements and yttrium. *Chem. Geol.* **82**, 159-186.
Zhang Y., Zhu L., Zeng X., Lin Y. (2004) The biogeochemical cycling of phosphorus in the upper ocean of the East China Sea *Estuarine, Coastal and Shelf Science* **60**, 369-379.

811 **Figure Captions**

812

813 **Figure 1:** Location and map of Ballynamintra Cave, County Waterford, Ireland. The circles with
814 the crosses indicate the location of the automatic water sampler in both plan (top panel)
815 and cross-section views (bottom two panels). The scale is the same for both the plan
816 view and cross section. Adapted from the original survey by Ryder et al. (1989).

817

818 **Figure 2:** A schematic of the automatic water sampling device used to collect daily-scale water
819 samples. The six aluminum vertical supports along the outside of the device are omitted
820 for clarity. The vertical supports connect the top, middle, and bottom disks but do not
821 intersect the freely rotating disks (shaded a darker grey in schematic) holding the sample
822 bottles. The device is also expanded vertically for clarity. The width of the apparatus at
823 the base is one meter, and the height is 500 cm.

824

825 **Figure 3a, b:** Time-series data extending from November 23, 2004, to January 22, 2006, for the
826 elements measured in this study. Data points suspected of contamination or below
827 detection limits are removed from the dataset. Two prolonged gaps in the record caused
828 by an unexpected voltage drop exist from February 17, 2005, to March 12, 2005, and
829 from July 23, 2005, to August 16, 2005. Drip rate as calculated from the volume of water
830 in each sampling bottle is shown, as are daily rainfall and calculated monthly water
831 excess (bottom panels). The numbers on the drip rate time-series correspond to the storm
832 hydrographs illustrated in figure 5 and discussed in the text.

833

834 **Figure 4:** Drip rate versus elemental concentration for the elements discussed in this research. The
835 top panel contains elements displaying a positive correlation with drip rate and the
836 bottom panel elements displaying a negative correlation. The lines are the best-fit power-

function regression lines for the various elements. For clarity, only the data points for Pb (top panel, squares), Mg (top panel, triangles), P (bottom panel, circles), and Na (bottom panel, circles) are shown. The correlations (r^2) for all the elements against drip rate are as follows: Mg = 0.41, Ca = 0.46, Sr = 0.36, Na = 0.43, Ba = 0.02, P = 0.61, Zn = 0.13, Cu = 0.30, Rb = 0.07, Pb = 0.46, U = 0.22, Y = 0.40, Cs = 0.63, Th = 0.54. Note the logarithmic scale used on the y-axis.

Figure 5: Drip rate versus elemental concentrations for Ca and Th at low drip rates. Lighter symbols represent samples collected from May 1 to July 23rd, 2004, the interval of time characterized by decreasing drip rates.

Figure 6: Drip rate versus time for four storm pulses (top panel) and the Mg^{2+} concentrations for the water during those same episodes (bottom panel). The hydrographs were chosen as the four most complete in the drip rate record (labeled in Fig. 3) as well as the ones corresponding with the most discrete, short-lived rain events. The beginning of the rising limb was designated as time zero, and the date corresponding to the minimum drip rate achieved just before the next drip rate increase was designated as time 100. The hydrographs were then resampled at 100 evenly spaced intervals in order to facilitate comparisons between the four events. The bold line is the average of all four drip rate hydrographs (top panel). Drip water Mg concentrations corresponding to the same four events are shown in the bottom panel, and the bold line is the averaged value for all four. At this drip site, Mg concentrations do not respond in a predictable way to variations in discharge caused by storm flow. Other trace elements behave equally unpredictably and are therefore not shown.

Figure 7: Mg, Ca, and Sr concentrations over the interval from May 1 to July 23rd, 2004, showing possible effects of dilution by condensation water. Concentrations for all three elements decrease synchronously until the sampled water reaches a [Ca^{2+}] of 1.09 mmol L^{-1}, which is the [Ca^{2+}] of water in equilibrium with ambient cave air PCO_2 and temperature. [Sr^{2+}] and [Mg^{2+}] are unaffected by the inferred condensation corrosion (i.e., calcite dissolution does not contribute these ions to the condensed water) so continue to decrease with increasing proportion of condensation water, diverging from the [Ca^{2+}] trend.

Figure 8: Adsorption potential plotted against exponent of the best-fit power-function regression line describing the relationship between drip rate and elemental concentrations as shown in Figure 4. The sea water-upper crust partition coefficient is from Taylor and McLennan (1985) and describes the likelihood of fractionation during sedimentary processing; the lower the value the more likely that the element is leached from seawater and included into fine-grained sediments. This is proportional to the strength of adsorption to colloidal material in the soil and drip water. The mean residence times of the elements in the ocean is also from Taylor and McClennan (1985) and similarly describes the adsorption potential. P is a nutrient element and resides in the oceans longer than would be expected simply by geochemical considerations due to scavenging and recycling by biota (Zhang et al., 2004).

Figure 9: Ternary diagram illustrating the relationship between Cu, Sr, and Zn concentrations of all the drip waters collected in this study. Circles with crosses indicate the position of soil and bedrock samples on the diagram. Filled circles indicate 'summer' samples, those that were collected between August 16, 2005, and September 10, 2005, corresponding to the period with elevated concentrations of many potentially colloidally-associated TE.

Bedrock defines a very clear end-member, and whereas while samples plot less closely to the soil sample collected and leached; several types of soil organic material may influence the TE signature rather than just one end member.

Figure 10: A) Average 'annual' trace element content from a stalagmite from Grotta di Ernesto, Italy (adapted from Borsato et al., 2007). The curves were created by stacking successive TE cycles observed in the stalagmite. Month 0 represents the centre of laminae visible in the stalagmite, and each month is then calculated as representing 1/12 of the distance between successive annual lamina. The values were normalized by dividing each data value by the average value for the entire assumed hydrological year. See Borsato et al. (2007) for a more in depth description of the data processing involved. **B)** Mean monthly TE concentration for the automatically collected drip water samples from BC. Month 0 is defined as the center of the spike in colloidally-associated TE (August 21 – September 19, 2005), and each 30-day period before or after is labeled accordingly as +/- x months from the peak. There were more 'months' before Month 0 than after in the drip water dataset; therefore no data exists for Months +5 and +6 (that would have corresponded with the period January 23 to March 23, 2006, had the record extended that far). The period of January 23 to March 23, 2005, was used as a replacement for the missing data to create a symmetrical record comparable with Panel A. The assumption was made that TE concentrations during the interval in question are comparable from 2005 to 2006.

Figure 11: Time series of the [TE] / [Ca^{2+}] ratios of various elements of particular interest versus time.

Figure 12: SEM image (top left image) of residue left on filter paper after the filtration of a monthly-collected water sample within BC. This sample was collected at a different drip

914 site than the automatic water sampler, but within the same chamber. The rest of the
915 images are EDX elemental mapping images of the same field of view. Clearly visible are
916 a large Al-rich, Ca-poor grain (upper center of images) and a P-rich, Al-poor particle
917 (upper left of images).
918
919 **Table 1:** Chemical data for water samples discussed in text. Elements are arranged in descending
920 order of mean concentration throughout the entire 13-month dataset (second column).
921 The third column is the exponent of the best-fit power function describing the
922 relationship between drip rate and the element. Also shown are mean residence times in
923 the oceans and the seawater-upper crust partition coefficients (both from Taylor and
924 McLennan, 1998); these same values are then shown relative to the values for Th for
925 each element, and the column labeled 'mean' is the mean of these two normalized values
926 per element. The 'adsorption potential index', is an index introduced in this research to
927 quantify how strongly a given element adheres to colloidal/particulate matter. This is
928 calculated by taking the logarithm of the mean value in the previous column; Th adheres
929 most strongly to particulates of all the elements considered here, and therefore has an
930 'adsorption potential' = 0.0. The final column is the rank of all the 'adsorption
931 potentials' listed here; Th adheres most strongly to colloidal material, and Na the least
932 strongly (~7.8 orders of magnitude less strongly than Th).
933

Figure 1

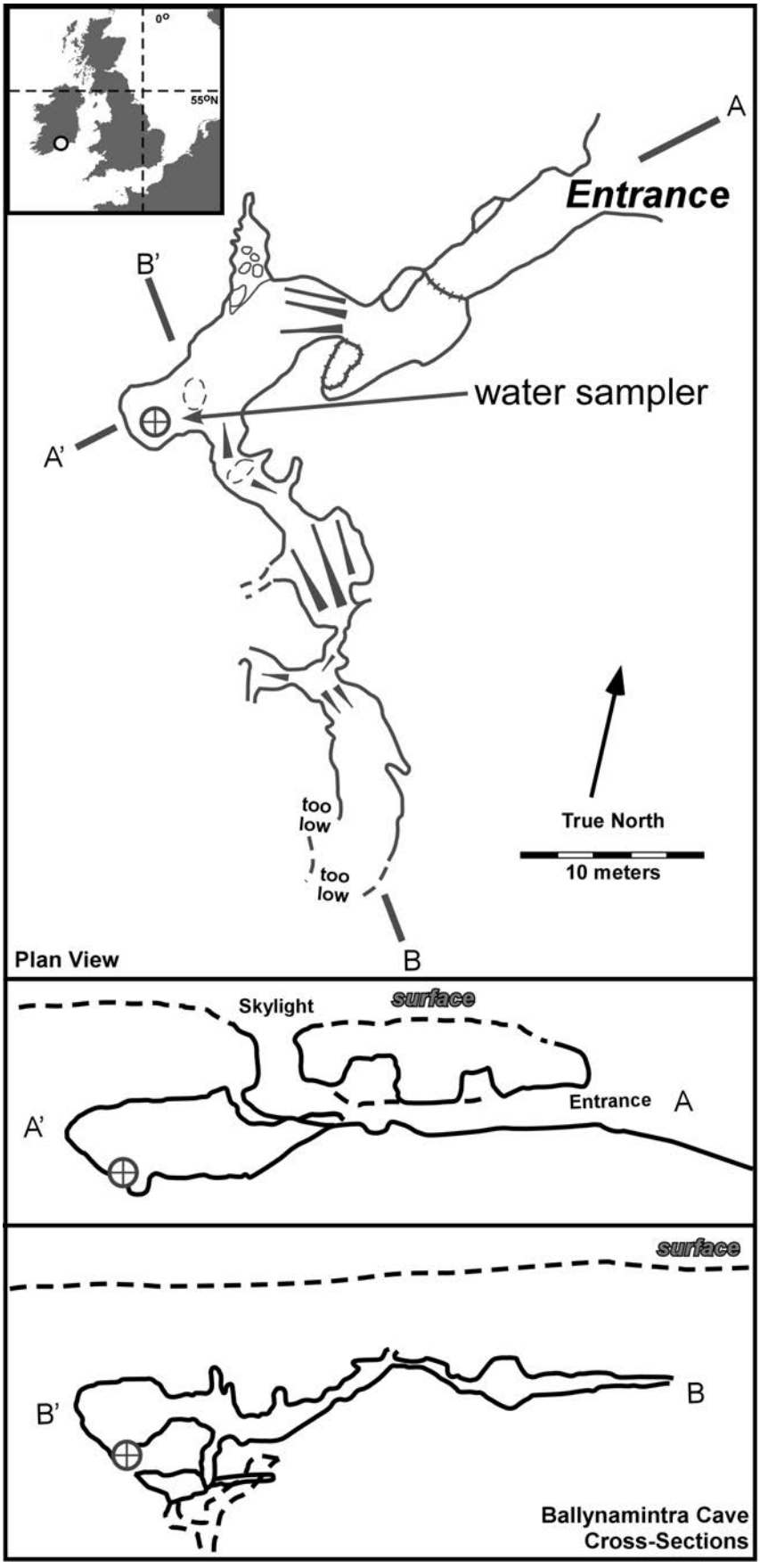
0°
55°N
A
Entrance
B'
water sampler
A'
too low
too low
True North
10 meters
B
Plan View
Skylight
surface
Entrance
A
A'
surface
B'
B
Ballynamintra Cave
Cross-Sections

Figure 2

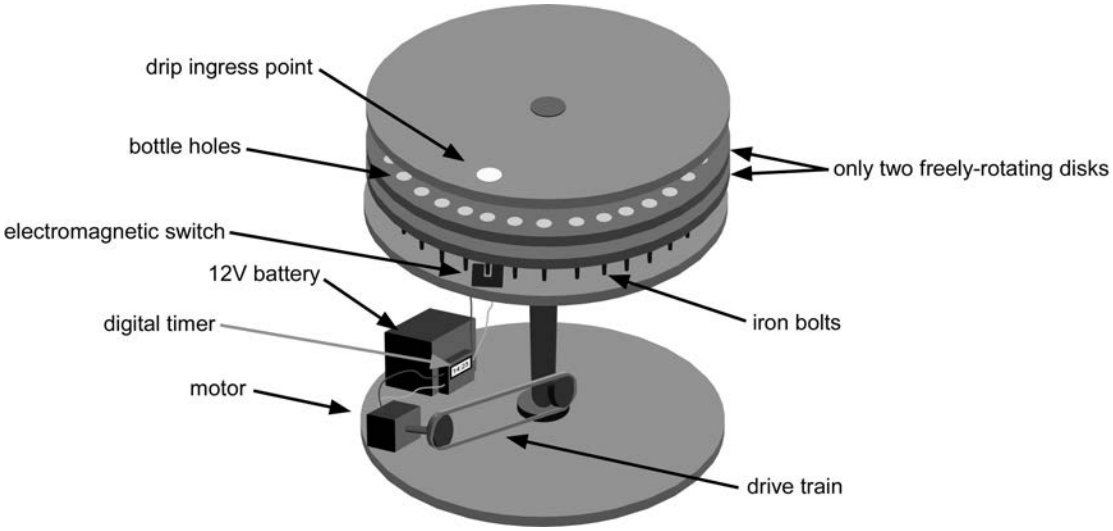
drip ingress point
bottle holes
electromagnetic switch
12V battery
digital timer
motor
only two freely-rotating disks
iron bolts
drive train

Figure 3a

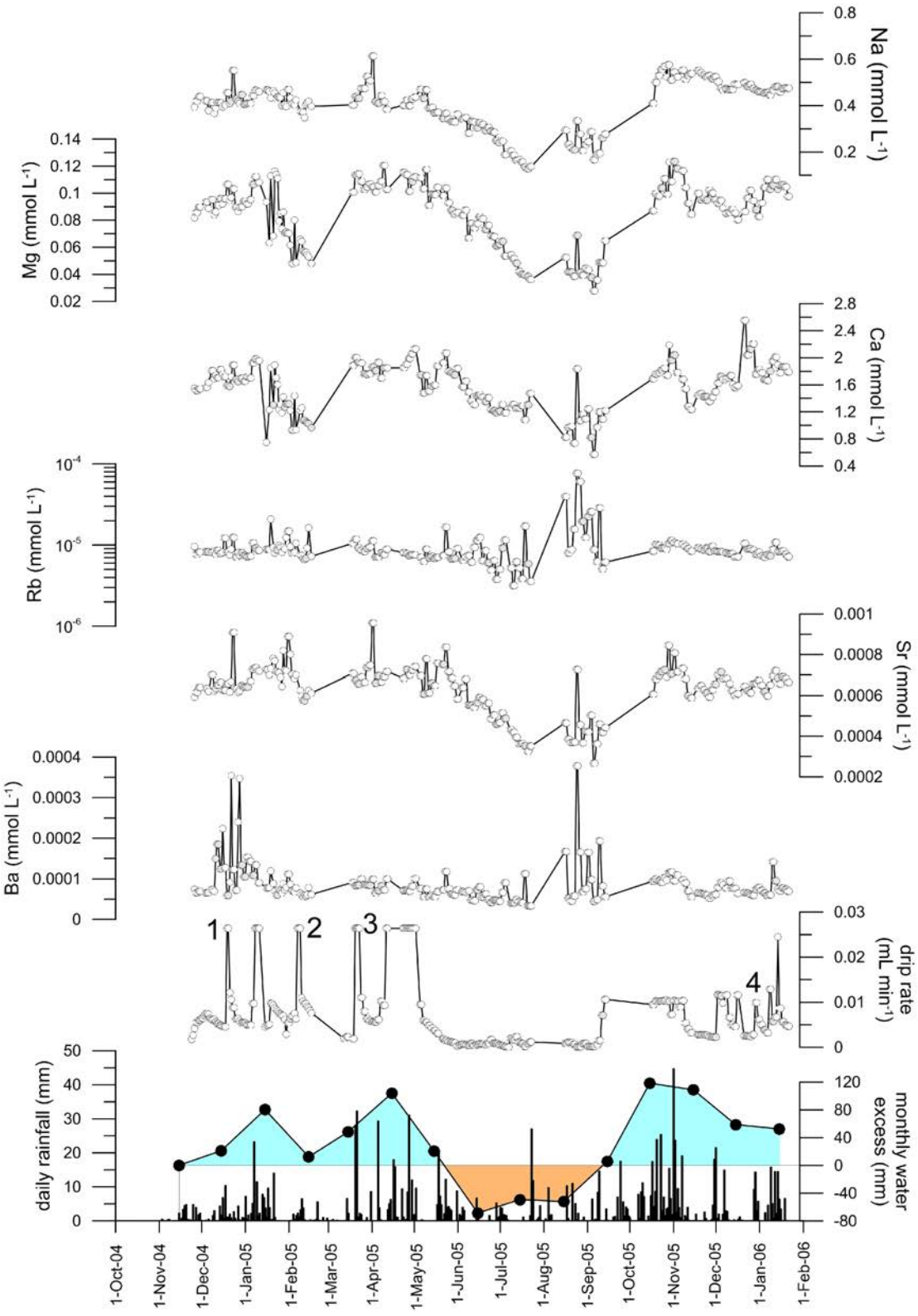
Na (mmol L-1)
0.8
0.6
0.4
0.2
Mg (mmol L-1)
0.14
0.12
0.1
0.08
0.06
0.04
0.02
Ca (mmol L-1)
2.8
2.4
2
1.6
1.2
0.8
0.4
Rb (mmol L-1)
10-4
10-5
10-6
Sr (mmol L-1)
0.001
0.0008
0.0006
0.0004
0.0002
Ba (mmol L-1)
0.0004
0.0003
0.0002
0.0001
0
1
2
3
4
drip rate (mL min-1)
0.03
0.02
0.01
0
daily rainfall (mm)
50
40
30
20
10
0
monthly water excess (mm)
120
80
40
0
-40
-80
1-Oct-04
1-Nov-04
1-Dec-04
1-Jan-05
1-Feb-05
1-Mar-05
1-Apr-05
1-May-05
1-Jun-05
1-Jul-05
1-Aug-05
1-Sep-05
1-Oct-05
1-Nov-05
1-Dec-05
1-Jan-06
1-Feb-06

Figure 3b

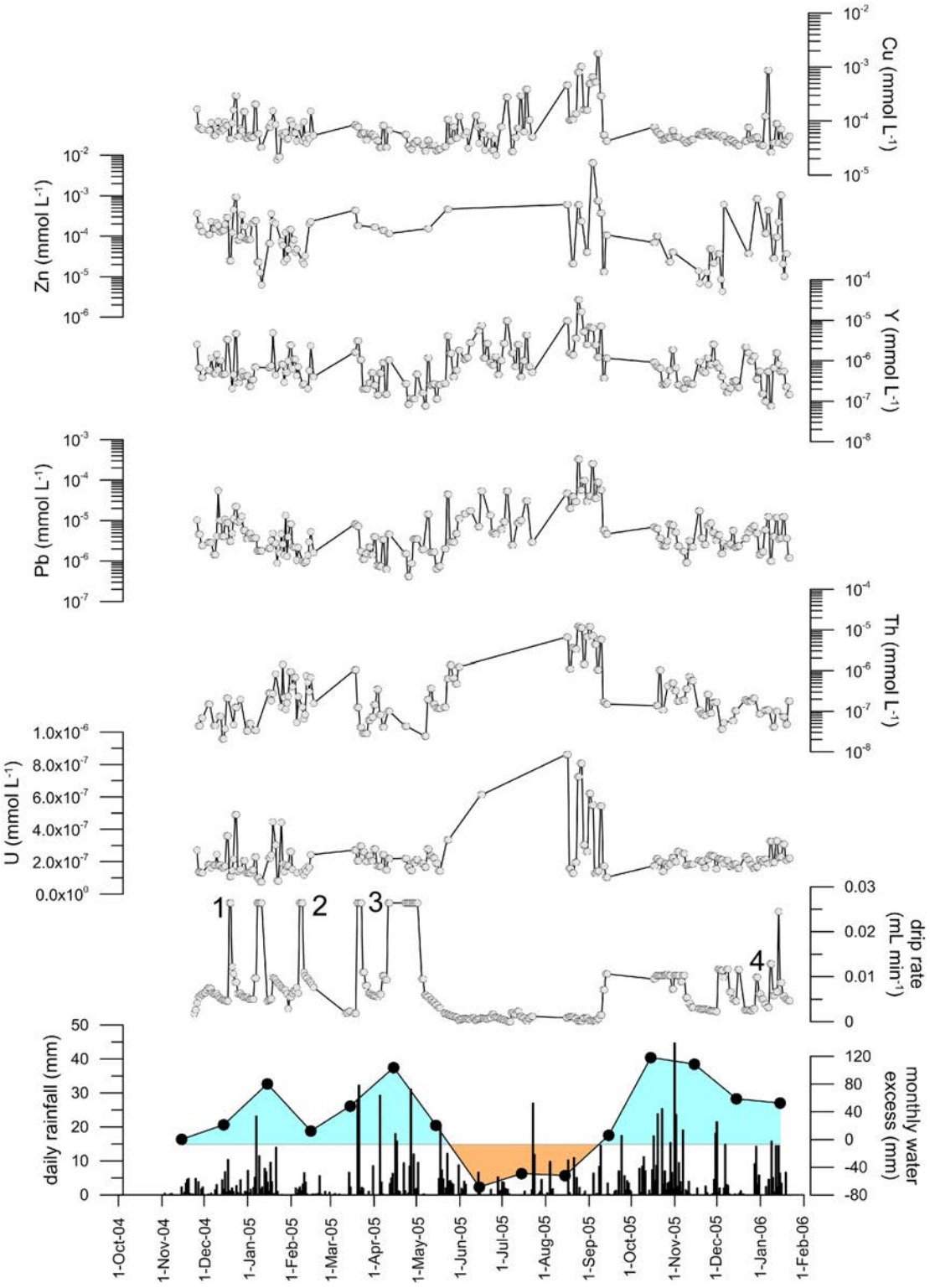
Cu (mmol L-1)
Zn (mmol L-1)
Y (mmol L-1)
Pb (mmol L-1)
Th (mmol L-1)
U (mmol L-1)
drip rate (mL min-1)
daily rainfall (mm)
monthly water excess (mm)
1
2
3
4
1-Oct-04
1-Nov-04
1-Dec-04
1-Jan-05
1-Feb-05
1-Mar-05
1-Apr-05
1-May-05
1-Jun-05
1-Jul-05
1-Aug-05
1-Sep-05
1-Oct-05
1-Nov-05
1-Dec-05
1-Jan-06
1-Feb-06

Figure 4

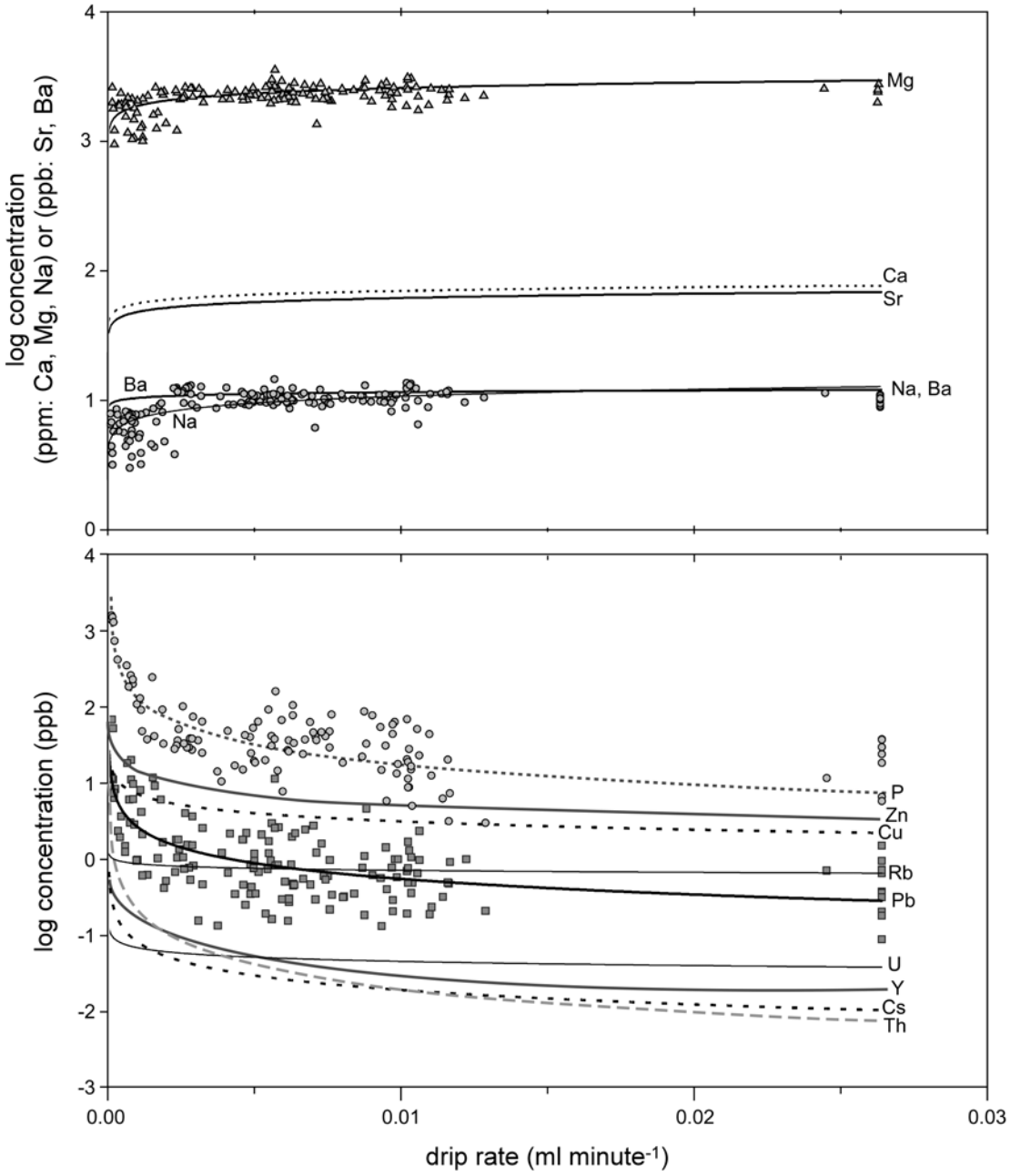
log concentration
(ppm: Ca, Mg, Na) or (ppb: Sr, Ba)
Mg
Ca
Sr
Ba
Na
Na, Ba
log concentration (ppb)
P
Zn
Cu
Rb
Pb
U
Y
Cs
Th
drip rate (ml minute-1)

Figure 5

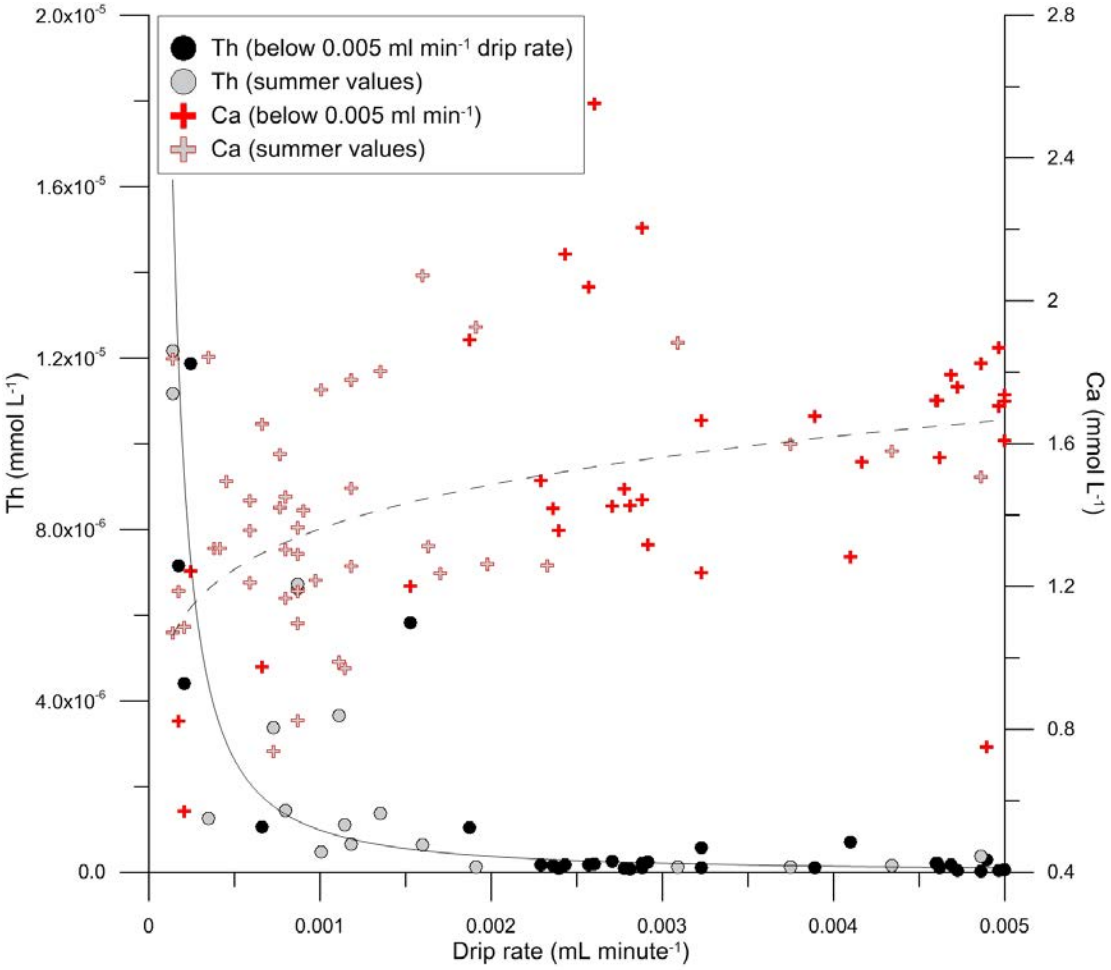
Th (below 0.005 ml min-1 drip rate)
Th (summer values)
Ca (below 0.005 ml min-1)
Ca (summer values)
Th (mmol L-1)
Ca (mmol L-1)
Drip rate (mL minute-1)
2.0x10-5
1.6x10-5
1.2x10-5
8.0x10-6
4.0x10-6
0.0
2.8
2.4
2
1.6
1.2
0.8
0.4
0
0.001
0.002
0.003
0.004
0.005

Figure 6

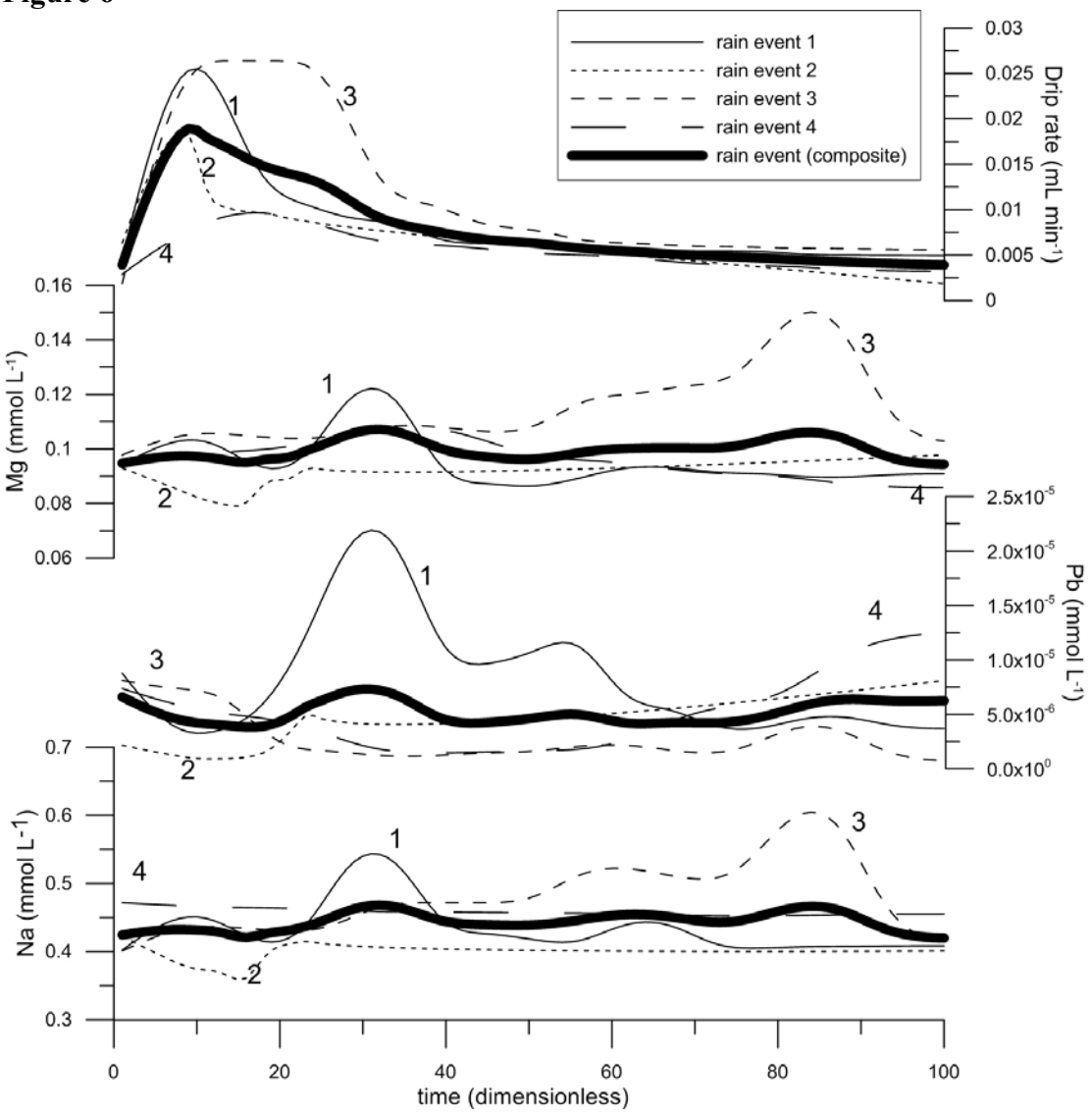
rain event 1
rain event 2
rain event 3
rain event 4
rain event (composite)
Drip rate (mL min-1)
0.03
0.025
0.02
0.015
0.01
0.005
0
Mg (mmol L-1)
0.16
0.14
0.12
0.1
0.08
0.06
Pb (mmol L-1)
2.5x10-5
2.0x10-5
1.5x10-5
1.0x10-5
5.0x10-6
0.0x10-0
Na (mmol L-1)
0.7
0.6
0.5
0.4
0.3
0
20
40
60
80
100
time (dimensionless)

Figure 7

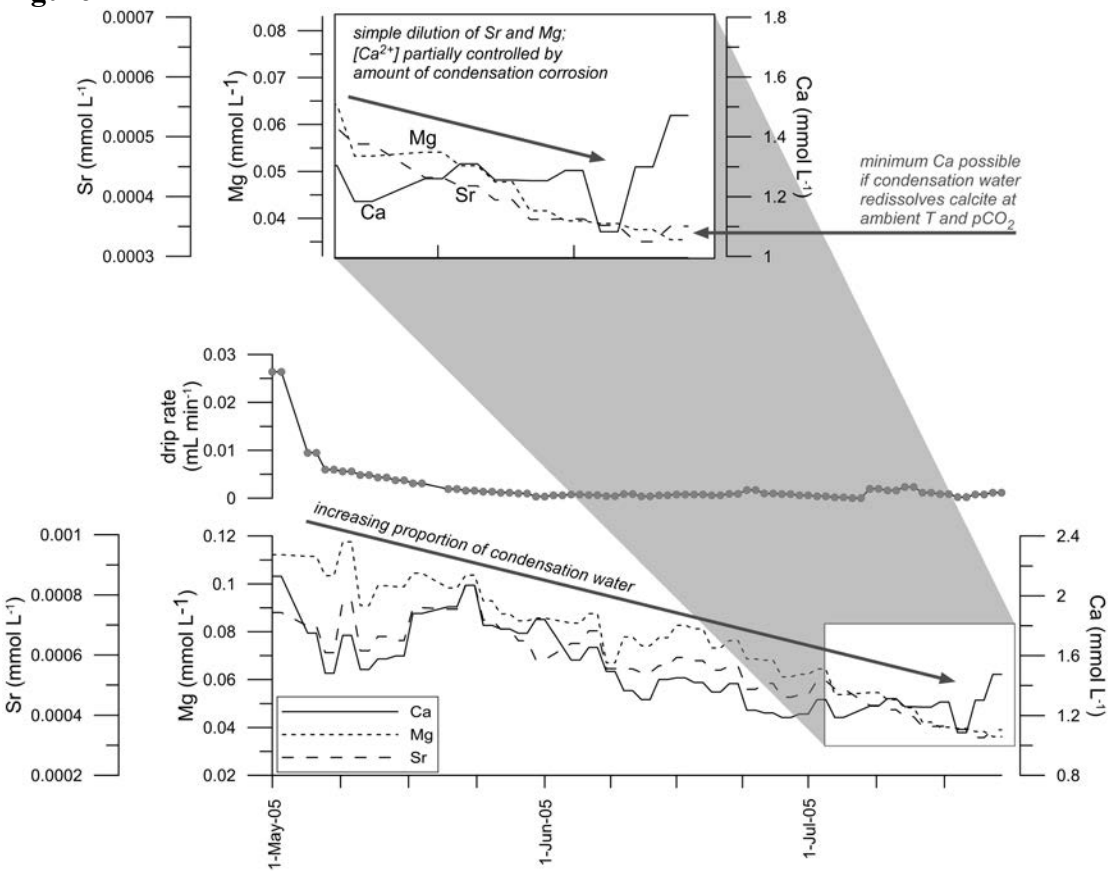

Figure 8

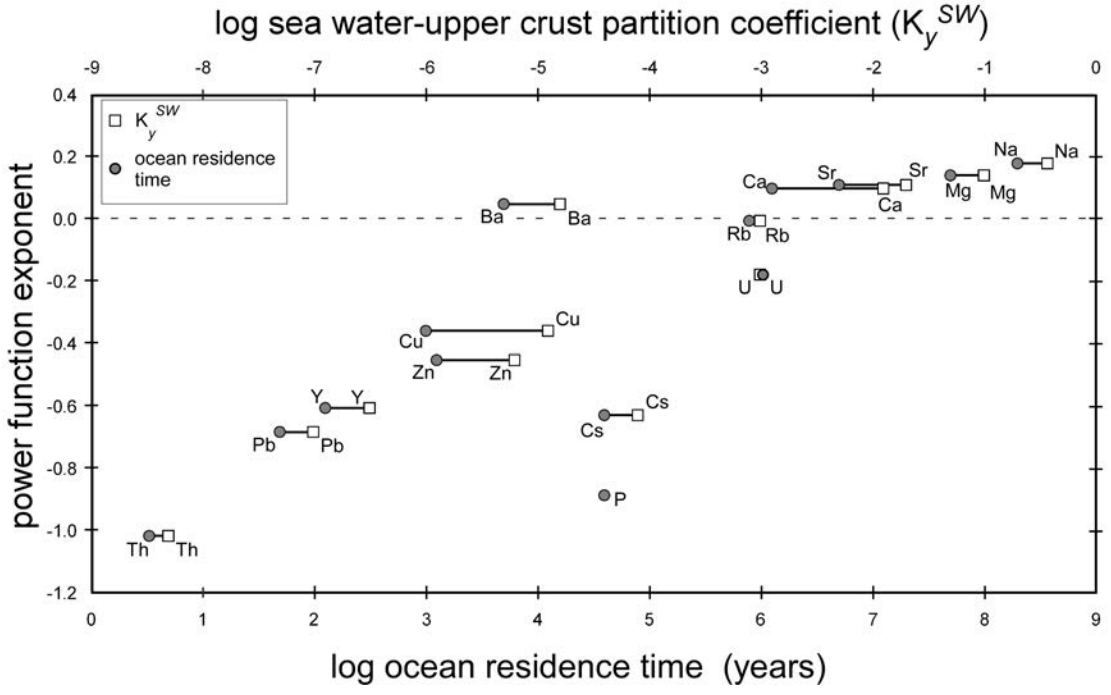

Figure 9

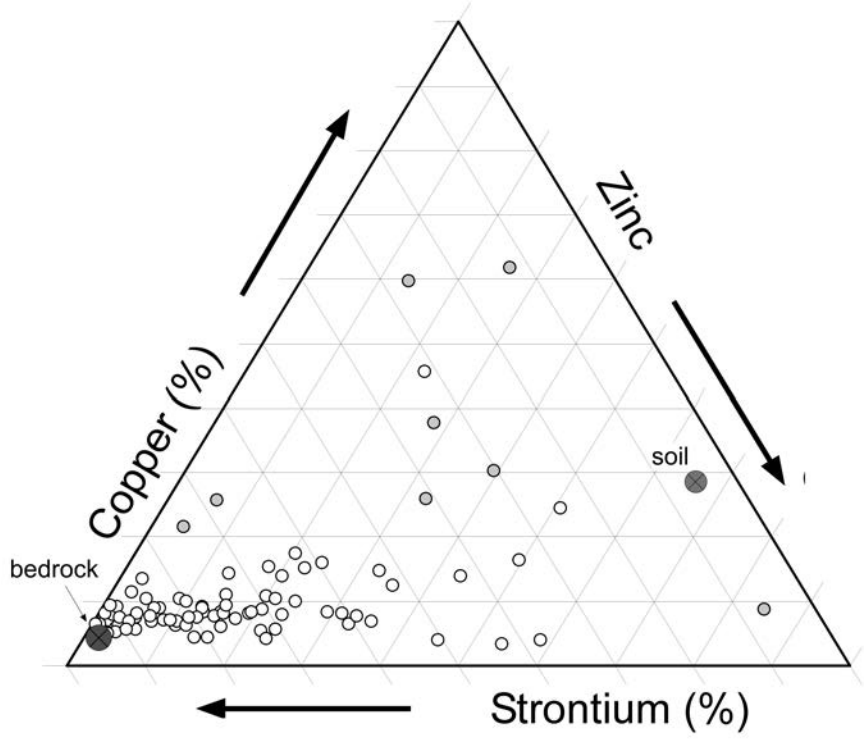

Figure 10

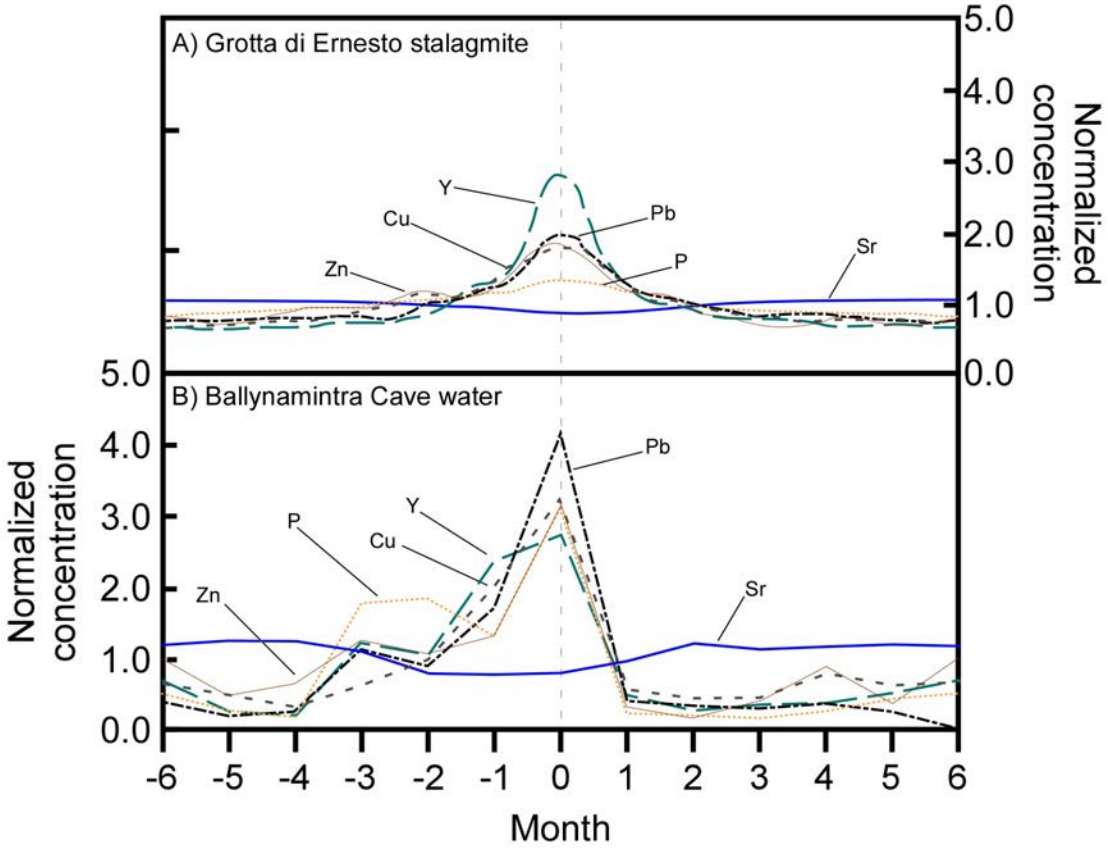

Figure 11

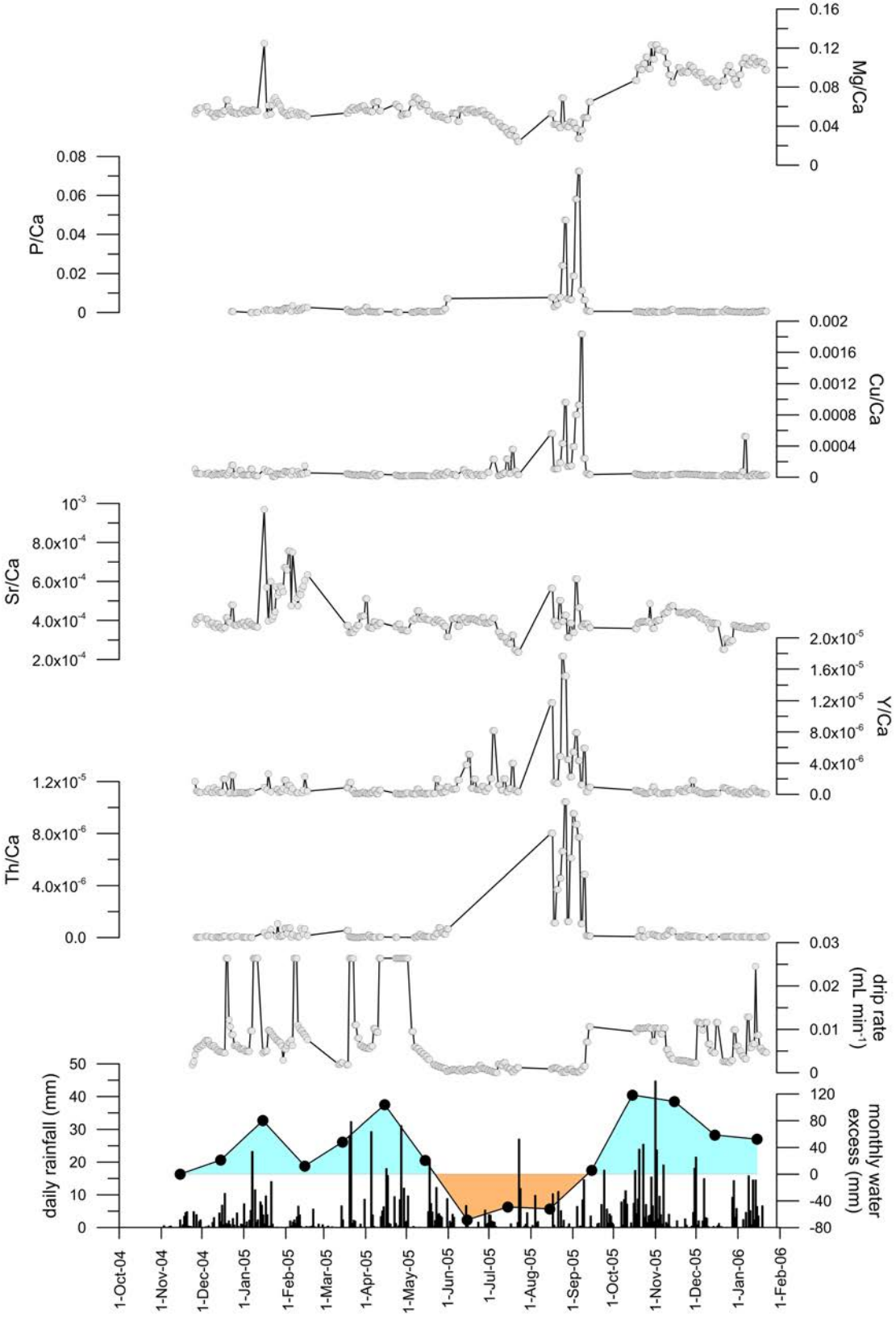
Mg/Ca
0.16
0.12
0.08
0.04
0
P/Ca
0.08
0.06
0.04
0.02
0
Cu/Ca
0.002
0.0016
0.0012
0.0008
0.0004
0
Sr/Ca
10-3
8.0x10-4
6.0x10-4
4.0x10-4
2.0x10-4
Y/Ca
2.0x10-5
1.6x10-5
1.2x10-5
8.0x10-6
4.0x10-6
0.0
Th/Ca
1.2x10-5
8.0x10-6
4.0x10-6
0.0
drip rate (mL min-1)
0.03
0.02
0.01
0
daily rainfall (mm)
50
40
30
20
10
0
monthly water excess (mm)
120
80
40
0
-40
-80
1-Oct-04
1-Nov-04
1-Dec-04
1-Jan-05
1-Feb-05
1-Mar-05
1-Apr-05
1-May-05
1-Jun-05
1-Jul-05
1-Aug-05
1-Sep-05
1-Oct-05
1-Nov-05
1-Dec-05
1-Jan-06
1-Feb-06

Figure 12

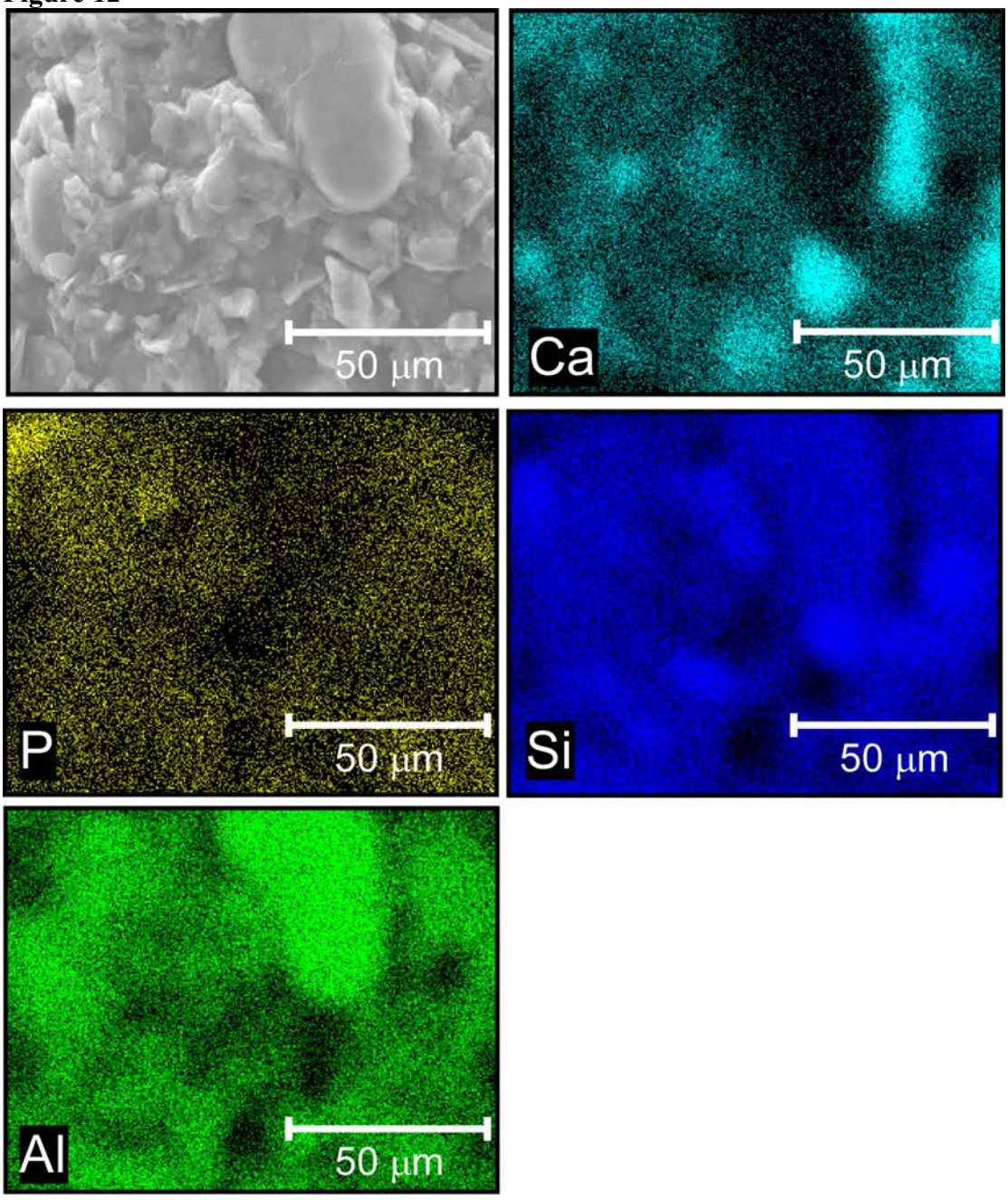

Table 1

Element	Mean concentration (ppb)	Concentration vs drip rate exponent	Residence time in oceans (yrs)	Sea water-upper crust partition coefficients (K_y^{SW})	Ocean residence time (relative to Th)	Sea water-upper crust partition coefficients (K_y^{SW}) (relative to Th)	Mean	'Adsorption potential index' strongest adsorption=0 (log mean)	Rank
Ca	63194.22	0.097	1.26E+06	1.26E−02	371535	2511886	1441711	6.2	11
Na	9178.09	0.176	2.00E+08	3.72E−01	58884366	74131024	66507695	7.8	14
Mg	2261.87	0.139	5.01E+07	1.00E−01	14791084	19952623	17371854	7.2	13
P	111.51	−0.889	3.98E+04	N/A	11749	N/A	11749	4.1	7
Sr	54.79	0.109	5.01E+06	2.00E−02	1479108	3981072	2730090	6.4	12
Zn	18.35	−0.454	1.26E+03	6.31E−06	372	1259	815	2.9	4
Ba	11.62	0.045	5.01E+03	1.58E−05	1479	3162	2321	3.4	6
Cu	7.16	−0.361	1.00E+03	1.26E−05	295	2512	1404	3.1	5
Pb	2.86	−0.685	5.01E+01	1.00E−07	15	20	17	1.2	2
Rb	0.85	−0.009	7.94E+05	1.00E−03	234423	199526	216975	5.3	9
Th	0.23	−1.020	3.39E+00	5.01E−09	1	1	1	0.0	1
Y	0.14	−0.606	1.26E+02	3.16E−07	37	63	50	1.7	3
Cs	0.07	−0.632	3.98E+04	7.94E−05	11749	15849	13799	4.1	8
U	0.06	−0.181	1.00E+06	1.00E−03	295121	199526	247324	5.4	10
Be	0.04								